

Maximum-Volume Nonnegative Matrix Factorization

Olivier Vu Thanh, Nicolas Gillis

Abstract—Nonnegative matrix factorization (NMF) is a popular data embedding technique. Given a nonnegative data matrix X , it aims at finding two lower dimensional matrices, W and H , such that $X \approx WH$, where the factors W and H are constrained to be element-wise nonnegative. The factor W serves as a basis for the columns of X . In order to obtain more interpretable and unique solutions, minimum-volume NMF (MinVol NMF) minimizes the volume of W . In this paper, we consider the dual approach, where the volume of H is maximized instead; this is referred to as maximum-volume NMF (MaxVol NMF). MaxVol NMF is identifiable under the same conditions as MinVol NMF in the noiseless case, but it behaves rather differently in the presence of noise. In practice, MaxVol NMF is much more effective to extract a sparse decomposition and does not generate rank-deficient solutions. In fact, we prove that the solutions of MaxVol NMF with the largest volume correspond to clustering the columns of X in disjoint clusters, while the solutions of MinVol NMF with smallest volume are rank deficient. We propose two algorithms to solve MaxVol NMF. We also present a normalized variant of MaxVol NMF that exhibits better performance than MinVol NMF and MaxVol NMF, and can be interpreted as a continuum between standard NMF and orthogonal NMF. We illustrate our results in the context of hyperspectral unmixing.

Index Terms—Volume-based regularization, nonnegative matrix factorization, identifiability, algorithms, hyperspectral unmixing.

I. INTRODUCTION

Let $X \in \mathbb{R}^{m \times n}$ be a flattened hyperspectral data cube, where m is the number of spectral bands and n is the number of pixels. Hyperspectral unmixing (HU) aims at finding the set of spectral signatures of the materials present in the scene, called endmembers, and their corresponding proportion in each pixel, called abundances. These endmembers and abundances are respectively stored in the matrices $W \in \mathbb{R}^{m \times r}$ and $H \in \mathbb{R}^{r \times n}$, where r is the number of endmembers. If we assume that interactions other than linear mixing are negligible, the data can be modeled as $X = WH + N$, where N is a noise matrix. Retrieving W and H is a challenging task that requires other assumptions than low-rank; in particular, nonnegative matrix factorization (NMF) [16] has shown to be effective for this task [5]. The nonnegativity assumption is motivated by the fact that the spectral reflectance of materials is nonnegative, and that the abundances of materials can only be additive. Another assumption is the minimum-volume criterion, originally thought by [13] and the so-called Craig's belief [8]. The idea is that, in the absence of pure

University of Mons, Rue de Houdain 9, 7000 Mons, Belgium. Emails: {olivier.vuthanh, nicolas.gillis}@umons.ac.be. The authors acknowledge the support by the European Research Council (ERC consolidator, eLinoR, no 101085607).

pixels (that is, pixels containing a single endmember), finding endmembers whose cone or convex hull tightly contains the data points retrieves the true endmembers. The minimum-volume criterion has also been used successfully in other applications, such as blind audio source separation [18], [26] and topic modeling [11], [10]. Regardless of the application, the minimum-volume criterion encourages interpretability of the features since they are close to the data points.

Maximum-volume NMF (MaxVol NMF), introduced in [23], maximizes the volume of H and can be interpreted as a dual approach of MinVol NMF [1]; see Section II for more details. However, to the best of our knowledge, its practical behavior, in particular on HU, has not been explored much. However, we will see that, in the presence of noise, MinVol NMF and MaxVol NMF behaves rather differently. In particular, MaxVol NMF is much more effective to extract a sparse factor H (that is, sparse abundances) and does not generate rank-deficient solutions.

Outline and contribution of the paper: In Section II, we motivate, introduce and analyze MaxVol NMF. In Section III, we propose two algorithms to solve MaxVol NMF. In Section IV, we present a normalized variant of MaxVol NMF that exhibits better performance than MinVol NMF and MaxVol NMF, which we illustrate in the context of HU in Section V. We conclude and discuss future works in Section VI.

II. MOTIVATION: MINVOL VS. MAXVOL NMF

In this section, we first highlight two weaknesses of MinVol NMF, and then introduce MaxVol NMF and how it avoids these two pitfalls.

A. Two weaknesses on MinVol NMF

In the absence of noise, MinVol NMF is defined as follows

$$\min_{W,H} \det(W^\top W) \text{ such that } X = WH, W \geq 0, H \in \Delta^{r \times n}, \quad (1)$$

where $\Delta^{r \times n}$ is the set of $r \times n$ matrices whose columns lies in the probability simplex, $\Delta^r = \{x \in \mathbb{R}^r \mid x \geq 0, e^\top x = 1\}$, e being the vector of all ones of appropriate dimension. This means that the simplex structure is imposed on the columns of H ; this is called the sum-to-one constraint in the HU literature. The quantity $\sqrt{\det(W^\top W)}/r!$ is the volume of the columns of W and the origin within the r -dimensional column space of W .

In practice, in the presence of noise, MinVol NMF needs to balance the volume and the data fitting terms, and the following optimization problem is often considered

$$\begin{aligned} \min_{W,H} \quad & \|X - WH\|_F^2 + \lambda \log \det(W^\top W + \delta I) \\ \text{s.t.} \quad & W \geq 0, H \in \Delta^{r \times n}, \end{aligned} \quad (2)$$

where λ is a penalty parameter, and δ is a small constant preventing $\log \det$ to be unbounded from below. The use of the $\log \det$ has algorithmic and practical advantages [11], [2].

Let us discuss two weaknesses of MinVol NMF. First, the MinVol criterion introduces a bias that can reduce the quality of the unmixing. Let us illustrate this with the Samson dataset that contains mostly three endmembers: water, soil and tree. The spectral signature of the water has a low magnitude relatively to the spectral signature of the soil and tree. Hence a bad estimation of the water spectral signature does not increase significantly the reconstruction error. Decreasing the norm of the spectral signature of the water is therefore an easy way to decrease the volume of W , and it can be done with only a slight increase in reconstruction error. This can be seen on Figure 1b, where the spectral signature of water (in red) for MinVol NMF with $\lambda = 1$ contains 24 zeros, while there should not be any zeros because there is not a wavelength at which water absorbs completely electromagnetic energy. Here, increasing λ will only worsen this behavior, e.g., 36 zeros for $\lambda = 50$.

Second, the sparsity of H in the decomposition is implicit and depends on the quality of the data. In the presence of noise, increasing the weight λ of the volume criterion will not necessarily increase the sparsity of H ; see Figure 1. When λ increases, the corresponding abundance map becomes a little bit crispier. Still, the improvement in terms of sparsity is not significant, and with a worse spectral signature for the water.

Now consider another, less noisy, dataset, the Moffett dataset. On Figure 2, we observe that the abundance map for NMF is not perfect, with mixed materials in the abundance maps. Adding the MinVol criterion with $\lambda = 1$ improves the decomposition and, as a consequence, the sparsity. Still, the water and tree extraction are not correct, as there are some detected water within the lands where it should in fact be trees. Increasing λ to 10 slightly improves this, but the water artifacts are still there. Increasing λ further does not improve the unmixing. With $\lambda = 50$, one of the columns of W collapses to zero. If a practitioner has some a priori knowledge on the sparsity of the decomposition, MinVol NMF cannot explicitly control sparsity, though sparsity is often desired in unmixing.

In this paper, we will see how MaxVol NMF preserves the spirit of MinVol NMF without the aforementioned weaknesses.

B. MaxVol NMF

Let us introduce MaxVol NMF through its equivalence with MinVol NMF in the exact case. Consider the NMF $X = \bar{W}\bar{H}$ where \bar{W} has full column rank. For any full column rank

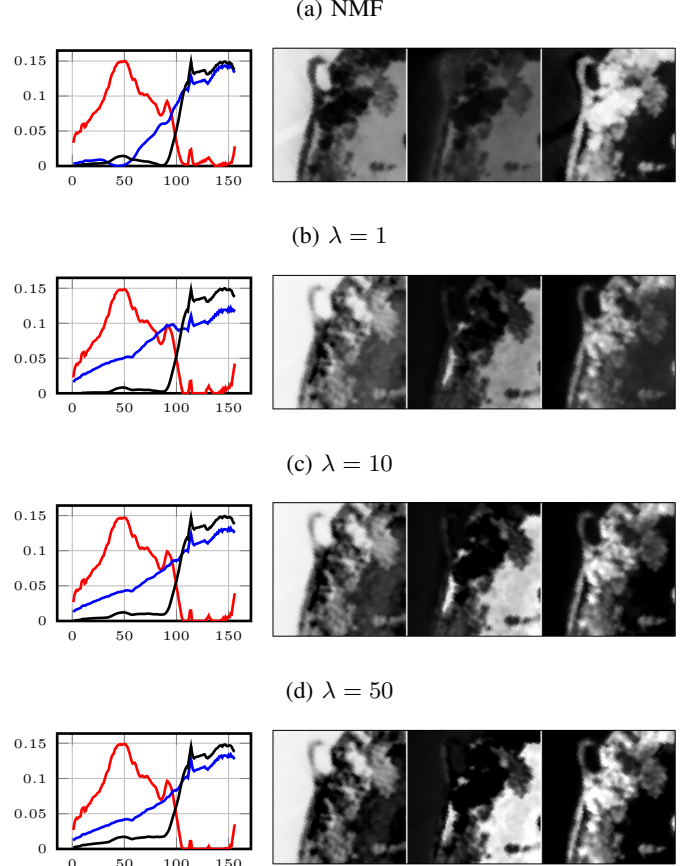


Figure 1: Abundance maps and normalized endmembers (from the left to the right: **water**, **soil** and **tree**) for MinVol on the Samson dataset with $\delta = 1$.

matrix W with the same column space as \bar{W} , there exists an invertible matrix Q such that $W = \bar{W}Q$. Then,

$$\det(W^\top W) = \det(Q^\top \bar{W}^\top \bar{W}Q) = \det(Q)^2 \det(\bar{W}^\top \bar{W}).$$

Minimizing $\det(W^\top W)$ is equivalent to minimizing $\det(Q)^2 \det(\bar{W}^\top \bar{W})$. Hence, given $X = \bar{W}\bar{H}$, computing the exact MinVol NMF of X is equivalent to solving

$$\min_Q \det(Q)^2 \quad \text{such that} \quad \bar{W}Q \geq 0, Q^{-1}\bar{H} \in \Delta^{r \times n}. \quad (3)$$

Minimizing the quantity $\det(Q)^2$ is equivalent to maximizing the quantity $\det(Q^{-2})$. To sum up, in the exact case, minimizing the volume of W is equivalent to maximizing the volume of H . This leads us to the MaxVol NMF formulation in the absence of noise:

$$\max_{W,H} \det(HH^\top) \quad \text{such that} \quad X = WH, W \geq 0, H \in \Delta^{r \times n}. \quad (4)$$

We now discuss the identifiability of MaxVol NMF, and its practical behavior.

C. Identifiability of MaxVol NMF

In the absence of noise, MaxVol NMF is just as identifiable as MinVol NMF [19], [12], under the same condition, defined as follows.

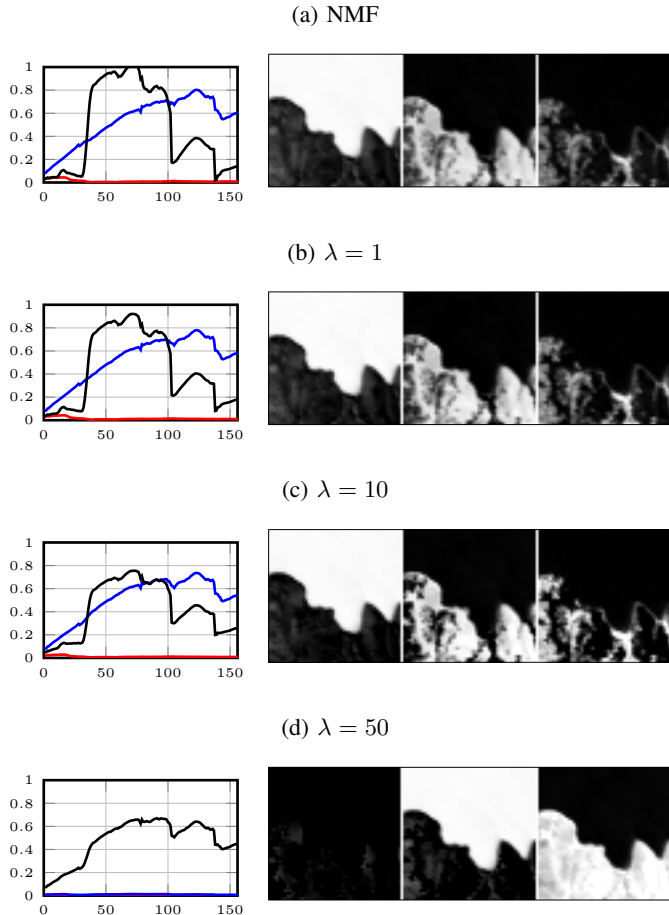


Figure 2: Abundance maps and normalized endmembers (from the left to the right: **water**, **soil** and **tree**, except for $\lambda = 50$ for MinVol on the Moffett dataset with $\delta = 0.1$).

Definition 1 (Sufficiently scattered condition - SSC): The matrix $H \in \mathbb{R}_+^{r \times n}$ is sufficiently scattered if the following two conditions are satisfied:

$$[\text{SSC1}] \quad \mathcal{C} = \{x \in \mathbb{R}_+^r \mid e^\top x \geq \sqrt{r-1} \|x\|_2\} \subseteq \text{cone}(H).$$

[\text{SSC2}] There does not exist any orthogonal matrix Q such that $\text{cone}(H) \subseteq \text{cone}(Q)$, except for permutation matrices.

The proof is almost exactly the same as the one for MinVol NMF. We report the proof here for completeness and because it provides insight on inner workings of MaxVol NMF.

Theorem 1: [23] Let $X = WH$ be a MaxVol NMF of X of size $r = \text{rank}(X)$, in the sense of (4). If H satisfies SSC as in Definition 1, then MaxVol NMF (W, H) of X is essentially unique.

Proof 1: Let $Q \in \mathbb{R}^{r \times r}$ be an invertible matrix such that (WQ^{-1}, QH) is another feasible solution of (4). There exists a right inverse H^\dagger such that $HH^\dagger = I$ because $\text{rank}(H) = r$. Since $e^\top H = e^\top$ and $e^\top QH = e^\top$ because (WQ^{-1}, QH) is feasible, we have

$$e^\top Q = e^\top QHH^\dagger = e^\top H^\dagger = e^\top HH^\dagger = e^\top.$$

Using again feasibility of (WQ^{-1}, QH) ,

$$QH \geq 0 \Leftrightarrow H^\top Q^\top \geq 0 \quad (5)$$

$$\Leftrightarrow Q(i,:)^\top \in \text{cone}^*(H) \quad (6)$$

$$\Leftrightarrow \text{cone}(Q^\top) \subseteq \text{cone}^*(H). \quad (7)$$

Since H satisfies SSC1, $\mathcal{C} \subseteq \text{cone}(H)$. By duality, $\text{cone}^*(H) \subseteq \mathcal{C}^*$, where $\mathcal{C}^* = \{y \in \mathbb{R}^r, e^\top y \geq \|y\|_2\}$ is the dual of \mathcal{C} . With (7), this implies that $\text{cone}(Q^\top) \subseteq \mathcal{C}^*$, that is,

$$Q(i,:)e \geq \|Q(i,:)\|_2 \text{ for } i = 1, \dots, r. \quad (8)$$

Therefore,

$$\begin{aligned} |\det(Q)| &\leq \prod_{i=1}^r \|Q(i,:)\|_2 \leq \prod_{i=1}^r Q(i,:)e \\ &\leq \left(\frac{\sum_{i=1}^r Q(i,:)e}{r} \right)^r = \left(\frac{e^\top Q e}{r} \right)^r = 1, \end{aligned} \quad (9)$$

where the first inequality is coming from the Hadamard's inequality, the second from (8), and the last one from the arithmetic-geometric mean inequality and that $e^\top Q = e^\top$.

Suppose now that (WQ^{-1}, QH) is also an optimal solution to (4). Then,

$$\begin{aligned} \det(QHH^\top Q^\top) &= \det(HH^\top) \\ \Leftrightarrow |\det(Q)|^2 \det(HH^\top) &= \det(HH^\top) \\ \Leftrightarrow |\det(Q)| &= 1. \end{aligned}$$

With $|\det(Q)| = 1$, all inequalities in (9) are equalities. Particularly, for all i , $Q(i,:)e = \|Q(i,:)\|_2 = 1$ and $|\det(Q)| = \prod_{i=1}^r \|Q(i,:)\|_2$, implying that Q^\top is orthogonal. By duality of (7) and using that the cone of any orthogonal matrix is self dual, we have that $\text{cone}(H) \subseteq \text{cone}(Q^\top)$. Finally, since H satisfies SSC2, Q^\top can only be a permutation matrix. \square

D. Behavior of MaxVol NMF

In the inexact case, we consider the following MaxVol NMF formulation:

$$\begin{aligned} \min_{W, H} \quad & f(W, H) := \frac{1}{2} \|X - WH\|_F^2 - \lambda \log \det(HH^\top + \delta I) \\ \text{s.t.} \quad & W \geq 0, H \in \Delta^{r \times n}. \end{aligned} \quad (10)$$

It should be noted that, unlike MinVol NMF, from an optimization perspective, the parameter δ in the logdet is not needed anymore. Maximizing the logdet will prevent H from being rank deficient. Still, we keep δ in our model because it has some physical meaning; see Section IV.

To understand the main difference between MinVol NMF and MaxVol NMF, consider the asymptotic case when λ goes to infinity. For MinVol NMF, W will converge to the all-zero matrix [17] for any $\delta > 0$, in order to minimize

$$\log \det(W^\top W + \delta I) = \sum_{i=1}^r \log(\sigma_i^2(W) + \delta),$$

where $\sigma_i(W)$ is the i th singular value of W . For MaxVol NMF, as λ goes to infinity, we can show that H converges to a matrix whose rows are mutually orthogonal, and such that

the l_2 norm of each row are as close to each other as possible. This is shown in Appendix A. Due to this result, and assuming n is a multiple of r (to simplify the presentation), that is, $n = dr$ for $d \in \mathbb{N}$, increasing λ in (10) will make HH^\top converge to a diagonal matrix whose elements are all equal to d . In other words, the rows of H will be mutually orthogonal while the simplex constraint on the columns of H imposes that $H(i, j) \in \{0, 1\}$. The squared l_2 norm of each row is equal to the number of non-zero elements in the corresponding row, d . From the HU point of view, one pixel will be assigned to only one material, this is a hard clustering where every cluster *must have the same size*. The clustering behavior of MaxVol NMF is interesting and offers more control over the sparsity of the decomposition than MinVol NMF. Also, maximizing the volume of H indirectly minimizes the volume of W without the drawback of potentially setting a useful endmember to zero due to its low reflectance or linear dependence with other endmembers. However, the fact that increasing λ leads to a clustering with clusters of the same size is a clear weakness. For this reason, we will introduce a normalized MaxVol NMF variant, N-MaxVol NMF, in Section IV that allows uneven clusters when the penalty parameter λ goes to infinity.

Figure 3 shows an experiment for the Samson data set. Increasing λ intensifies the clustering, until a hard clustering is achieved with $\lambda = 50$. Increasing λ removes some of the false positives for water, but not all of them. The pixels that are wrongly assigned to water are actually pixels that are in the shadow, which makes their reflectance low. The simplex structure of H prevents the model from assigning pixels to their correct endmember but to one with lower magnitude (in this case, water). Also, the improvement of the abundance map of the water is at the cost of a hard clustering, while a soft clustering would be preferable to properly unmix soil and tree. In Section IV, we will present an improved variant of MaxVol NMF to mitigate this issue.

Remark 1: About the results in Figure 3:

- λ is tuned using [21], where convergence is assumed when the relative difference of the objective function between two successive iterates is below 10^{-4} , and where the maximum variation of λ is capped to 10%.
- In Section III we show two different algorithms to solve MaxVol NMF. The abundance maps displayed on Figure 3 are the same regardless of the used algorithm, except for $\lambda = 50$ where the adaptive gradient method crashes, probably due to some numerical issues. The ADMM based algorithm still works well with $\lambda = 50$.

III. SOLVING MAXVOL NMF

The most common strategy to solve matrix factorizations problems such as MaxVol NMF (10) is to use block coordinate descent schemes. Here, we consider two blocks: W and H . Compared to MinVol NMF (2), the main difficulty in solving (10) holds in the term $-\lambda \logdet(\cdot)$.

For MinVol NMF, since $X \rightarrow \logdet(X)$ is concave, it is possible to derive a quadratic majorizer relatively to W whose gradient is Lipschitz continuous, and then use gradient descent on this majorizer [11], [17]. In fact, the first-order

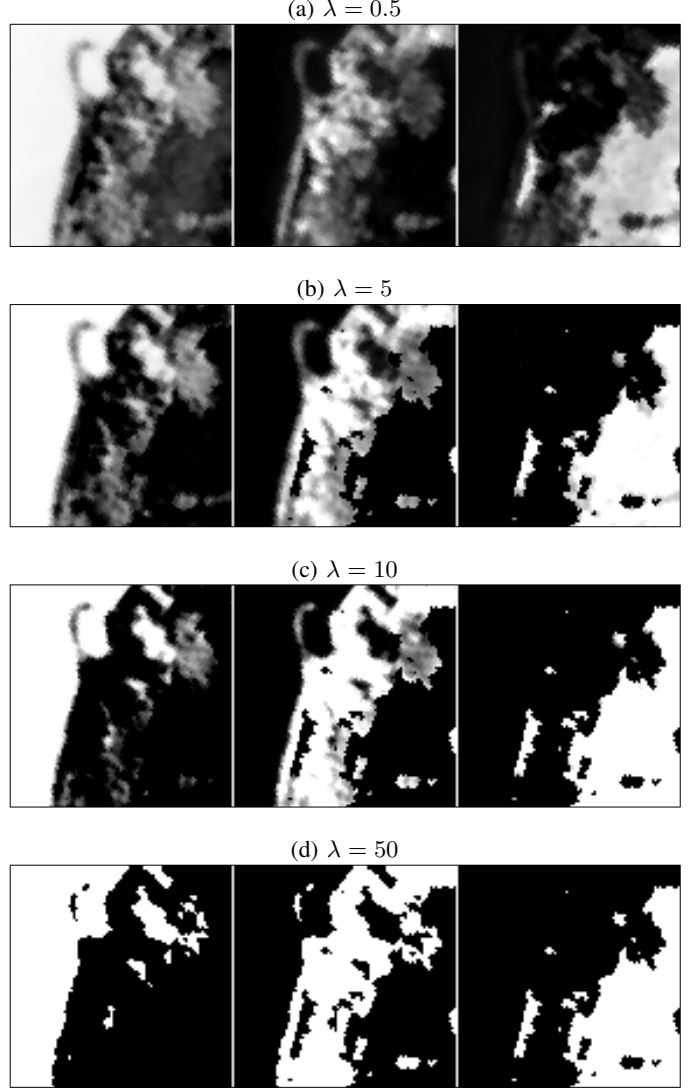


Figure 3: Abundance maps of MaxVol NMF on Samson, depending on λ .

Taylor approximation $\logdet(X)$ at the current iterate provides such a majorizer.

Unfortunately, $-\logdet(\cdot)$ is not concave, which prevents from using the aforementioned updating strategy for (10). In this section, we propose two algorithms to solve (10). The first algorithm in Section III-A is adapted from [20]. Its core idea is to approximate the local Lipschitzness by using the previous iterate and to compute the corresponding Lipschitz gradient descent. The second algorithm is based on the Alternating Direction Method of Multipliers (ADMM). The reason we introduce two algorithms is as follows: although ADMM will work better on average, we will be able to adapt the first algorithm to our new proposed N-MaxVol NMF model from Section IV.

A. Adaptive accelerated gradient descent

Our first proposed algorithm for (10) relies on [20, Alg. 2]. This algorithm uses the previous iterate to approximate the

local Lipschitzness and derive an appropriate step size. The previous iterate is also used to induce some extrapolation. The only knowledge that is needed from the objective function is its gradient. It should be noted that [20, Alg. 2] is only designed to update all variables at once. In our case, it would mean that $[W^\top, H] \in \mathbb{R}^{r \times (m+n)}$ should be updated all at once. Most gradient-based algorithms for constrained matrix factorization are using a two block alternating strategy, performing several updates on W and then several updates on H . By doing so, computational savings are possible by precomputing some quantities that remain unchanged during the update of one block (e.g., XH^\top and HH^\top when updating W). We will follow this common two-block strategy and, all we need are the gradients of MaxVol NMF (10):

$$\begin{aligned}\nabla f(W) &= \frac{\partial f}{\partial W}(W) = (WH - X)H^\top, \\ \nabla f(H) &= \frac{\partial f}{\partial H}(H) = W^\top(WH - X) - 2\lambda(HH^\top + \delta I)^{-1}H.\end{aligned}$$

Our adaptation of [20, Alg. 2] with a two-block strategy is given in Algorithm 1.

Remark 2: The adaptive part is mostly useful for the update of H . In order to update W , which requires to solve a convex nonnegative least squares problem, any other algorithm could be used instead of the **while** loop in Algorithm 1.

B. Alternating direction method of multipliers (ADMM)

Let us introduce the variable $Y = HH^\top \in \mathbb{R}^{r \times r}$ and let $\Lambda \in \mathbb{R}^{r \times r}$ be the Lagrange multipliers corresponding to this constraint, and consider the following ADMM reformulation of (10):

$$\begin{aligned}\min_{W, H, Y, \Lambda} \quad & \mathcal{L}(W, H, Y, \Lambda) := \frac{1}{2}\|X - WH\|_F^2 \\ & - \lambda \logdet(Y + \delta I) + \langle Y - HH^\top, \Lambda \rangle \\ & + \frac{\rho}{2}\|Y - HH^\top\|_F^2\end{aligned}\tag{11}$$

s.t. $W \geq 0, H \in \Delta^{r \times n}$.

ADMM consists of the following updates [4]:

$$W^{k+1} = \underset{W \geq 0}{\operatorname{argmin}} \mathcal{L}(W, H^k, Y^k, \Lambda^k)\tag{12}$$

$$H^{k+1} = \underset{H \geq \Delta^{r \times n}}{\operatorname{argmin}} \mathcal{L}(W^{k+1}, H, Y^k, \Lambda^k)\tag{13}$$

$$Y^{k+1} = \underset{Y}{\operatorname{argmin}} \mathcal{L}(W^{k+1}, H^{k+1}, Y, \Lambda^k)\tag{14}$$

$$\Lambda^{k+1} = \Lambda^k + \rho(Y^{k+1} - H^{k+1}H^{k+1\top})\tag{15}$$

a) *Updating W :* Like in Section III-A, the update for W can be computed through any algorithm for constrained convex problems, as (12) is equivalent to

$$W^{k+1} = \underset{W \geq 0}{\operatorname{argmin}} \frac{1}{2}\|X - WH^k\|_F^2.$$

Here we propose to use TITAN [15], an extrapolated first-order algorithm with convergence guarantees, like in [24]. The resulting update for W^{k+1} is detailed in Algorithm 2

b) *Updating H :* We propose two ways of updating H . The first one consists of solving directly (13) with the adaptive accelerated gradient descent algorithm described

Algorithm 1: Adgrad2

```

Input: data matrix  $X \in \mathbb{R}^{m \times n}$ , initial factors
 $W_o \in \mathbb{R}_+^{m \times r}$  and  $H_o \in \Delta^{r \times n}$ 
1  $\Gamma_{W_o} = \|H_o H_o^\top\|, \gamma_{W_o} = \Gamma_{W_o}^{-1}, \theta_W = \Theta_W =$ 
 $10^9, \bar{W}_o = W_o, \bar{W} = W = [W_o - 10^{-6}\nabla f(W_o)]_+$ 
2  $\Gamma_{H_o} = \|W_o^\top W_o\|, \gamma_{H_o} = \Gamma_{H_o}^{-1}, \theta_H = \Theta_H =$ 
 $10^9, \bar{H}_o = H_o, \bar{H} = H = [H_o - 10^{-6}\nabla f(H_o)]_{\Delta^{r \times n}}$ 
3 for  $k = 1, 2, \dots$  do
4   while stopping criteria not satisfied do
5      $\gamma_W =$ 
6        $\min \left( \gamma_{W_o} \sqrt{1 + \frac{\theta_W}{2}}, \frac{\|\bar{W} - \bar{W}_o\|_F}{2\|\nabla f(\bar{W}) - \nabla f(\bar{W}_o)\|_F} \right)$ 
7      $\Gamma_W =$ 
8        $\min \left( \Gamma_{W_o} \sqrt{1 + \frac{\Theta_W}{2}}, \frac{\|\nabla f(\bar{W}) - \nabla f(\bar{W}_o)\|_F}{2\|\bar{W} - \bar{W}_o\|_F} \right)$ 
9      $W = [\bar{W} - \gamma_W \nabla f(\bar{W})]_+$ 
10     $\theta_W = \gamma_W / \gamma_{W_o}, \Theta_W = \Gamma_W / \Gamma_{W_o}$ 
11     $\bar{W}_o = \bar{W}$ 
12     $\bar{W} = W + \frac{1 - \sqrt{\gamma_W \Gamma_W}}{1 + \sqrt{\gamma_W \Gamma_W}}(W - W_o)$ 
13     $W_o = W$ 
14     $\gamma_{W_o} = \gamma_W, \Gamma_{W_o} = \Gamma_W$ 
15   while stopping criteria not satisfied do
16      $\gamma_H =$ 
17        $\min \left( \gamma_{H_o} \sqrt{1 + \frac{\theta_H}{2}}, \frac{\|\bar{H} - \bar{H}_o\|_F}{2\|\nabla f(\bar{H}) - \nabla f(\bar{H}_o)\|_F} \right)$ 
18      $\Gamma_H =$ 
19        $\min \left( \Gamma_{H_o} \sqrt{1 + \frac{\Theta_H}{2}}, \frac{\|\nabla f(\bar{H}) - \nabla f(\bar{H}_o)\|_F}{2\|\bar{H} - \bar{H}_o\|_F} \right)$ 
20      $H = [\bar{H} - \gamma_H \nabla f(\bar{H})]_{\Delta^{r \times n}}$ 
21      $\theta_H = \gamma_H / \gamma_{H_o}, \Theta_H = \Gamma_H / \Gamma_{H_o}$ 
22      $\bar{H}_o = \bar{H}$ 
23      $\bar{H} = H + \frac{1 - \sqrt{\gamma_H \Gamma_H}}{1 + \sqrt{\gamma_H \Gamma_H}}(H - H_o)$ 
24      $H_o = H$ 
25      $\gamma_{H_o} = \gamma_H, \Gamma_{H_o} = \Gamma_H$ 

```

Algorithm 2: Update of W with TITAN

```

Input:  $\alpha_1, X, H^k, W, W_o$ 
Output:  $W$ 
1  $L_W = \|H^k H^{k\top}\|$ 
2 while stopping criteria not satisfied do
3    $\alpha_0 = \alpha_1$ 
4    $\alpha_1 = \frac{1}{2}(1 + \sqrt{1 + 4\alpha_0^2})$ 
5    $\beta = \frac{\alpha_0 - 1}{\alpha_1}$ 
6    $\bar{W} = W + \beta(W - W_o)$ 
7    $W_o = W$ 
8    $W = [\bar{W} + \frac{1}{L_W}(XH^\top - \bar{W}H^k H^{k\top})]_+$ 

```

in Section III-A. The second one consists of deriving a non-Euclidean gradient method. We derive a Bregman surrogate of $H \rightarrow \mathcal{L}(W^{k+1}, H, Y^k, \Lambda^k) := \mathcal{L}(H)$ and update H by minimizing this surrogate. The main motivation to use such a surrogate is that there does not exist a Lipschitz surrogate of \mathcal{L}

relatively to H . The gradient of $H \rightarrow \mathcal{L}(W^{k+1}, H, Y^k, \Lambda^k)$ is clearly not Lipschitz continuous because the gradient of $\|Y - HH^\top - \delta I\|_F^2$ relatively to H is cubic. Although $H \rightarrow \mathcal{L}(H)$ is not L -smooth, using the framework of [3], we can show that it is smooth relatively to the quartic norm kernel proposed in [9].

Definition 2 (Bregman distance): Given a convex function h , dubbed a distance kernel, the corresponding Bregman distance is defined as

$$D_h(x, y) = h(x) - h(y) - \langle \nabla h(y), x - y \rangle.$$

Note that D_h is not a proper distance as it is asymmetric.

Definition 3 (Relative smoothness [3]): We say that a differentiable function $f : \mathbb{R}^{r \times n} \rightarrow \mathbb{R}$ is L -smooth relatively to the distance kernel h if there exists $L > 0$ such that for every $X, Y \in \mathbb{R}^{r \times n}$,

$$f(X) \leq f(Y) + \langle \nabla f(Y), X - Y \rangle + LD_h(X, Y).$$

If f is twice differentiable, L -smoothness relatively to h is equivalent to

$$\nabla^2 f(X)[U, U] \leq L \nabla^2 h(X)[U, U] \quad \forall X, U \in \mathbb{R}^{r \times n},$$

where $\nabla^2 f(X)[U, U]$ denotes the second derivative of f at X in the direction U .

First, we focus on the relative smoothness of the quartic term. According to [9] we have

$$\begin{aligned} \frac{1}{2} \|Y - HH^\top\|_F^2 := g(H) &\leq g(H^k) + \langle \nabla g(H^k), H - H^k \rangle \\ &\quad + D_h(H, H^k), \end{aligned} \quad (16)$$

where $\nabla g(H^k) = 2(H^k H^{k\top} - Y)H^k$, and $h(H) = \frac{\alpha}{4}\|H\|_F^4 + \frac{\sigma}{2}\|H\|_F^2$ with $\alpha = 6$ and $\sigma = 2\|Y\|_2$. Substituting (16) in (11),

$$\begin{aligned} \mathcal{L}(H) \leq u_{H^k}(H) &:= \frac{1}{2}\|X - WH\|_F^2 - \langle HH^\top, \Lambda \rangle \\ &\quad + \rho \langle \nabla g(H^k), H \rangle + \rho h(H) - \rho \langle \nabla h(H^k), H \rangle + C_H \end{aligned} \quad (17)$$

where C_H is a constant relatively to H . Let us compute the second directional derivative of u_{H^k} ,

$$\begin{aligned} \nabla^2 u_{H^k}(H)[U, U] &= \langle (W^\top W - 2\Lambda^\top)U, U \rangle + \rho\sigma\|U\|_F^2 \\ &\quad + \rho\alpha(\|H\|_F^2\|U\|_F^2 + 2\langle H, U \rangle^2) \\ &\leq \rho\alpha(\|H\|_F^2\|U\|_F^2 + 2\langle H, U \rangle^2) \\ &\quad + (\|W^\top W - 2\Lambda^\top\|_2 + \rho\sigma)\|U\|_F^2 \\ &= \nabla^2 \left(\frac{\tilde{\alpha}}{4}\|H\|_F^4 + \frac{\tilde{\sigma}}{2}\|H\|_F^2 \right) [U, U], \end{aligned} \quad (18)$$

where $\tilde{\alpha} = \rho\alpha$ and $\tilde{\sigma} = \rho\sigma + \|W^\top W - 2\Lambda^\top\|_2$. From (18) and (17), $H \rightarrow \mathcal{L}(H)$ is 1-smooth relatively to the kernel $\tilde{h} : H \rightarrow \frac{\tilde{\alpha}}{4}\|H\|_F^4 + \frac{\tilde{\sigma}}{2}\|H\|_F^2$. More explicitly,

$$\mathcal{L}(H) \leq u_{H^k}(H^k) + \langle \nabla u_{H^k}(H^k), H - H^k \rangle + D_{\tilde{h}}(H, H^k).$$

The update for H is then obtained by minimizing the

aforementioned surrogate

$$\begin{aligned} H^{k+1} &= \operatorname{argmin}_{H \in \Delta^{r \times n}} \left\{ \langle \nabla u_{H^k}(H^k), H \rangle + \tilde{h}(H) - \langle \nabla \tilde{h}(H^k), H \rangle \right\}, \\ &= \operatorname{argmin}_{H \in \Delta^{r \times n}} \left\{ t_k(H) := \tilde{h}(H) - \langle Q^k, H \rangle \right\}, \end{aligned} \quad (19)$$

where $Q^k = \nabla \tilde{h}(H^k) - \nabla u_{H^k}(H^k)$. This is equivalent to the Bregman proximal iteration map described in [9] with a step size equal to 1.

Corollary 1: The solution of (19) is of the form

$$H^{k+1} = \frac{1}{\tilde{\alpha}\|H^{k+1}\|_F^2 + \tilde{\sigma}}[Q^k - e\nu^\top]_+,$$

where $\nu \in \mathbb{R}^n$.

Proof 2: Consider the Lagrangian of (19)

$$\mathcal{L}_{t_k}(H, \Lambda, \nu) = t_k(H) - \langle H, \Lambda \rangle + \langle H^\top e - e, \nu \rangle$$

where $\Lambda \in \mathbb{R}_+^{r \times n}$ and $\nu \in \mathbb{R}^n$. According to the KKT optimality conditions:

$$H^{k+1} \in \Delta^{r \times n}, \quad (20)$$

$$\langle \Lambda^*, H^{k+1} \rangle = 0, \quad (21)$$

$$\nabla t_k(H^{k+1}) - \Lambda^* + e\nu^{*\top} = 0, \quad (22)$$

$$\Leftrightarrow \begin{cases} H^{k+1} \in \Delta^{r \times n}, \\ \langle \nabla \tilde{h}(H^{k+1}) - Q^k + e\nu^{*\top}, H^{k+1} \rangle = 0, \end{cases} \quad (23)$$

$$\Leftrightarrow \begin{cases} \langle \nabla \tilde{h}(H^{k+1}) - Q^k + e\nu^{*\top}, H^{k+1} \rangle = 0, \\ \nabla \tilde{h}(H^{k+1}) - Q^k + e\nu^{*\top} \geq 0, \end{cases} \quad (24) \quad (25)$$

where (24) is coming from substituting (22) in (21), and (25) is coming from the fact that $\Lambda^* \geq 0$. First, combining (24) and (25), we have

$$(\nabla \tilde{h}(H^{k+1}) - Q^k + e\nu^{*\top}) \circ H^{k+1} = 0, \quad (26)$$

where \circ is the Hadamard product. For all p in $1, \dots, r$, for all j in $1, \dots, n$,

1) if $Q^k(p, j) - \nu_j^* < 0$, $\nabla \tilde{h}(H^{k+1})(p, j) - (Q^k(p, j) - \nu_j^*) > 0$ because $\nabla \tilde{h}(H) = (\tilde{\alpha}\|H\|_F^2 + \tilde{\sigma})H \geq 0$, then (26) $\Rightarrow H^{k+1}(p, j) = 0$,

2) if $Q^k(p, j) - \nu_j^* = 0$, $\nabla \tilde{h}(H^{k+1})(p, j) = (\tilde{\alpha}\|H^{k+1}\|_F^2 + \tilde{\sigma})H^{k+1}(p, j)$ so (26) $\Rightarrow H^{k+1}(p, j) = 0$,

3) if $Q^k(p, j) - \nu_j^* > 0$, $\nabla \tilde{h}(H^{k+1})(p, j) = (\tilde{\alpha}\|H^{k+1}\|_F^2 + \tilde{\sigma})H^{k+1} > 0$ by (25), then (26) $\Rightarrow \nabla \tilde{h}(H^{k+1})(p, j) - (Q^k(p, j) - \nu_j^*) = 0 \Leftrightarrow H^{k+1}(p, j) = \frac{Q^k(p, j) - \nu_j^*}{\tilde{\alpha}\|H^{k+1}\|_F^2 + \tilde{\sigma}}$.

In the end, $H^{k+1} = \frac{1}{\tilde{\alpha}\|H^{k+1}\|_F^2 + \tilde{\sigma}}[Q^k - e\nu^{*\top}]_+$. \square

In particular, ν in Corollary 1 is such that $e^\top [Q^k - e\nu^\top]_+ = (\tilde{\alpha}\|H^{k+1}\|_F^2 + \tilde{\sigma})e^\top \in \mathbb{R}^n$ since $e^\top H^{k+1} = e^\top$. In other words, $[Q^k - e\nu^\top]_+$ projects Q on a scaled probability simplex where the scaling is equal to $\tilde{\alpha}\|H^{k+1}\|_F^2 + \tilde{\sigma}$. How do we find ν since it depends on H^{k+1} ? We propose to solve this inexactly with a simple fixed point algorithm where $\|H^{k+1}\|_F^2$ is the variable to optimize. The idea is that when $\|H^{k+1}\|_F^2$ is fixed, ν has a closed form solution. So for a fixed $\|H^{k+1}\|_F^2$ we compute ν , then we update $\|H^{k+1}\|_F^2$ according to the new ν and repeat this process. The algorithm is described

in Algorithm 3. When $\|H^{k+1}\|_F^2$ is fixed, there are several algorithms that can compute exactly ν . In [14], the proposed algorithm requires to sort the entries of each column of Q^k . The main computational cost of this algorithm is this sorting. Once the sorting is completed, ν is found just by computing n times the max between r entries, which is linear. There exist faster algorithms like [7] that do not rely on sorting. However, note that Q^k is not changing in Algorithm 3. Hence, using [14] to compute ν in Algorithm 3 only has a linear complexity if Q^k is sorted only once before the **while** loop. In our code, ϵ is fixed to 10^{-6} and the **while** loop cannot exceed 100 iterations.

Algorithm 3: Algorithm to update H in (19)

Input: $Q^k, \tilde{\alpha}, \tilde{\sigma}$
init: $\|H^{k+1}\|_F^2, \nu$
Output: H^{k+1}

- 1 **while** $\frac{\|H^{k+1}\|_F^2 - \left\| \frac{1}{\tilde{\alpha}\|H^{k+1}\|_F^2 + \tilde{\sigma}} [Q^k - e\nu^\top]_+ \right\|_F^2}{\|H^{k+1}\|_F^2} > \epsilon$ **do**
- 2 compute ν such that

$$\frac{1}{\tilde{\alpha}\|H^{k+1}\|_F^2 + \tilde{\sigma}} [Q^k - e\nu^\top]_+ \in \Delta^{r \times n}$$
- 3 update $\|H^{k+1}\|_F^2$ to $\left\| \frac{1}{\tilde{\alpha}\|H^{k+1}\|_F^2 + \tilde{\sigma}} [Q^k - e\nu^\top]_+ \right\|_F^2$
- 4 $H^{k+1} = \frac{1}{\tilde{\alpha}\|H^{k+1}\|_F^2 + \tilde{\sigma}} [Q^k - e\nu^\top]_+$

c) *Updating Y :* The ADMM update of Y^{k+1} is

$$Y^{k+1} = \underset{Y \succ -\delta I}{\operatorname{argmin}} -\lambda \operatorname{logdet}(Y + \delta I) + \langle Y, \Lambda \rangle + \frac{\rho}{2} \|Y - HH^\top\|_F^2.$$

Consider the change of variable $Z = Y + \delta I$,

$$\begin{aligned} Y^{k+1} + \delta I &= \underset{Z \succ 0}{\operatorname{argmin}} -\lambda \operatorname{logdet}(Z) \\ &\quad + \frac{\rho}{2} \left\| Z - \left(HH^\top + \delta I - \frac{1}{\rho} \Lambda \right) \right\|_F^2. \end{aligned} \quad (27)$$

According to [25, Lemma 2.1], (27) has a closed form solution which is

$$\Phi_{\frac{\lambda}{\rho}}^+ \left(HH^\top + \delta I - \frac{1}{\rho} \Lambda \right)$$

where $\Phi_\gamma^+(x) = \frac{1}{2}(\sqrt{x^2 + 4\gamma} + x)$ and for a symmetric A with an eigen value decomposition $A = PDP^\top$ and $D = \operatorname{Diag}(d)$, $\Phi_\gamma^+(A) = P \operatorname{Diag}(\Phi_\gamma^+(d)) P^\top$ where $\Phi_\gamma^+(d)$ is applied element-wise. In the end,

$$Y^{k+1} = \Phi_{\frac{\lambda}{\rho}}^+ \left(HH^\top + \delta I - \frac{1}{\rho} \Lambda \right) - \delta I.$$

C. Comparison of the two algorithms

We now compare the two proposed algorithms for MaxVol NMF, both on synthetic and real datasets. The results are averaged over 10 runs and are presented on Figure 5. For the synthetic dataset, W is drawn following a uniform distribution in $[0, 1]$ and H is such that each of its column is drawn following a Dirichlet distribution where the concentration parameters are all equal to 0.2. The input matrix is $X = WH$. A different X is drawn at each run. The compared algorithms are Adgrad2 (Section III-A), ADMM (Section III-B) and

ADMM+Adgrad. ADMM+Adgrad has the same formulation as in (11), but the update for H (13) is performed using the adaptive gradient descent method instead of minimizing the proposed Bregman surrogate. Regardless of the dataset and of the algorithm, the number of iterations is fixed to 500, the number of inner iterations (that is, the number of times H is updated before updating W , and vice-versa) is fixed to 20, λ and δ are fixed to 1. In Figure 5, on both synthetic data and Moffett, ADMM with $\rho = 0.01$ has the best convergence speed and the lowest error. Still on synthetic data and Moffett, the proposed Bregman surrogate provides a nice approximation of the original ADMM formulation (11). For equal ρ 's, ADMM always converges faster and to a lower error than ADMM+Adgrad. This experimentally justifies our choice for the use of a Bregman surrogate to update H in the ADMM formulation of MaxVol NMF. However, this is at the cost of a higher computation time, due to Algorithm 3, as it can be seen in the reported average times in Table I. One can always increase the tolerance threshold ϵ in Algorithm 3, but should remain careful. Let us increase ϵ to 10^{-3} . The computation time of ADMM with $\rho = 0.01$ is greatly reduced, as a run on the synthetic dataset only lasts 2.44s on average. However, for $\rho = 0.1$ the algorithm diverges, as it can be seen on Figure 4, and the computation time is increased to 6.90s on average. Finally, ADMM is not always better than Adgrad2, like with Samson on Figure 5c. Reasons as to why one algorithm would be better than the other, and designing effective algorithms for MaxVol NMF are questions of further research.

Algorithm	Times (s)
Adgrad2	3.67
ADMM+Adgrad $\rho = 0.01$	2.88
ADMM+Adgrad $\rho = 0.1$	2.29
ADMM $\rho = 0.01$	5.33
ADMM $\rho = 0.1$	23.5

Table I: Average time per run on synthetic datasets.

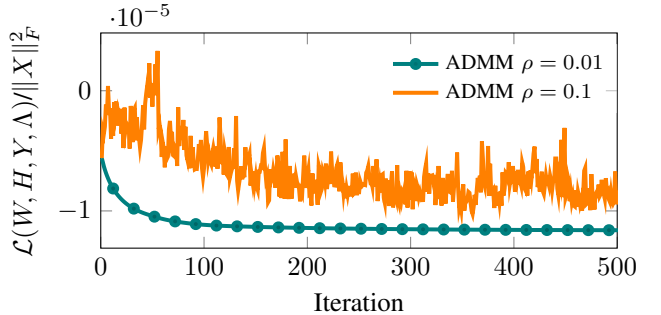


Figure 4: ADMM on synthetic dataset with $\epsilon = 10^{-3}$

IV. NORMALIZED MAXVOL NMF (N-MAXVOL NMF)

In Section II-B, we explained that a main drawback of MaxVol (10) is its bias towards clusters of the same size when λ increases. Here, we introduce a normalized variant

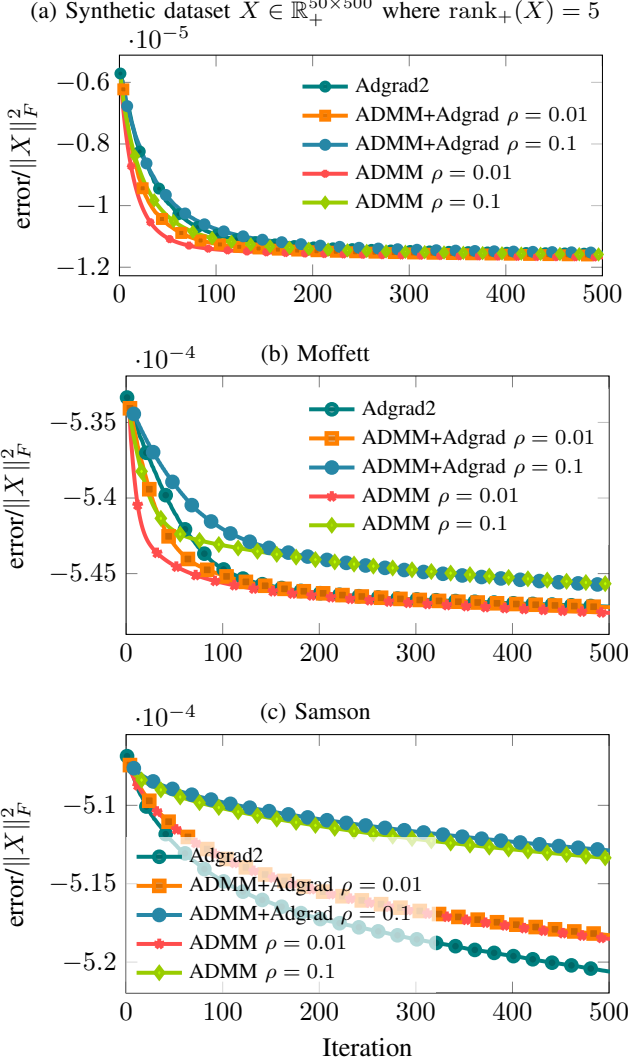


Figure 5: Comparison of algorithms for MaxVol NMF on various datasets

of MaxVol NMF to alleviate this issue, by maximizing the volume of the row-wise normalized H , denoted \tilde{H} :

$$\begin{aligned} \min_{W, H, \tilde{H}} \quad & f(W, H) := \frac{1}{2} \|X - WH\|_F^2 - \lambda \log \det(\tilde{H} \tilde{H}^\top + \delta I) \\ \text{s.t.} \quad & W \geq 0, H \geq 0, \tilde{H} = S^{-1}H, \\ & \text{where } S = \text{Diag}(\|H(1, :)\|_2, \dots, \|H(r, :)\|_2). \end{aligned} \quad (28)$$

Let us explain why this model will not be biased towards even clusterings. As λ increases, one can show that $\tilde{H} \tilde{H}^\top$ converges to the identity; see Appendix B. In other words, increasing λ acts in favor of mutually orthogonal rows of H . Unlike MaxVol NMF, the norm of the rows of H can take any non-zero value since it is $\tilde{H} \tilde{H}^\top$ that converges to the identity and not HH^\top . In fact, N-MaxVol NMF can be viewed as a continuum between NMF and Orthogonal NMF (ONMF), where ONMF requires $HH^\top = I_r$ and is equivalent to a weighted variant of spherical k-means [22].

It is possible to control the range of the volume criterion

via δ . For $\delta > 0$,

$$\log \det(\tilde{H} \tilde{H}^\top + \delta I) \in [\log((r + \delta)\delta^{r-1}), r \log(1 + \delta)],$$

where the minimum and maximum are respectfully reached when $\tilde{H} \tilde{H}^\top = ee^\top$ and $\tilde{H} \tilde{H}^\top = I$; see Appendix B. The parameter δ hence controls how large the volume of \tilde{H} can be, while λ balances the reconstruction error and the volume criterion. By increasing δ , the range is reduced, as it can be seen on Figure 6. With respect to λ and the reconstruction error, it is then harder to give more importance to the volume term in the objective. In the context of HU, δ can be seen as a mixture tolerance parameter, while λ is a noise level estimation parameter.

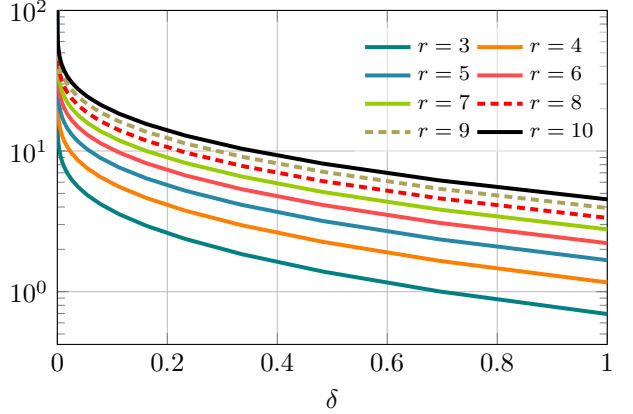


Figure 6: Value of $r \log(1 + \delta) - \log(1 + r\delta^{-1}) - r \log \delta$ depending on δ for various r 's.

Another feature of N-MaxVol NMF is the removal of the simplex structure on H . Recall that the simplex structure is not without loss of generality. In HU for instance, if there are two pure pixels of the same material but one of them receives more light than the other, then a perfect unmixing would require a different endmember for each. In other words, the simplex structure might require a larger rank.

In spite of the benefits the normalized variant brings, we “lose” two aspects of the vanilla MaxVol NMF. The most notable one is the identifiability. It remains unknown if N-MaxVol NMF is identifiable or not. We also lose the possibility to solve N-MaxVol NMF with the same ADMM formulation that we used for MaxVol NMF. We could not find a kernel that would provide us with a Bregman surrogate. Even if we did, the considered Bregman surrogate would then need to be nice enough to be easily solvable. We will therefore solve it with the adaptive accelerated gradient descent method.

A. Solving N-MaxVol NMF

We solve N-MaxVol NMF (28) with the adaptive accelerated gradient descent method, introduced in Section III-A, and for which we only need to know the gradient which we provide in this section. The algorithm is exactly the same as Algorithm 1, except for the projected gradient step in Algorithm 1 that should be replaced by $H = [\tilde{H} - \gamma_H \nabla f(\tilde{H})]_+$, where f is the objective function, because there is no simplex structure

in the normalized variant. It remains to compute the gradient of f in (28) relatively to H . Knowing that

$$\begin{aligned} \frac{\partial \tilde{H}(k,:)}{\partial H(k,j)} &= \begin{pmatrix} -\frac{H(k,1)H(k,j)}{\|H(k,:)\|^3} \\ \vdots \\ \frac{\|H(k,:)\|^2 - H(k,j)^2}{\|H(k,:)\|^3} \\ \vdots \\ -\frac{H(k,n)H(k,j)}{\|H(k,:)\|^3} \end{pmatrix}^\top \\ &= \frac{1}{\|H(k,:)\|^3} (\|H(k,:)\|^2 e_j^\top - H(k,j)H(k,:)), \end{aligned}$$

and using the chain rule, we have that

$$\begin{aligned} \frac{\partial \log \det(\tilde{H}\tilde{H}^\top + \delta I)}{\partial H(k,j)} &= \left\langle \frac{\partial \log \det(\tilde{H}\tilde{H}^\top + \delta I)}{\partial \tilde{H}}, \frac{\partial \tilde{H}}{\partial H(k,j)} \right\rangle \\ &= \left\langle 2(\tilde{H}\tilde{H}^\top + \delta I)^{-1}\tilde{H}, \frac{E_{k,j}}{\|H(k,:)\|} - \frac{H(k,j)}{\|H(k,:)\|^3}e_k H(k,:) \right\rangle \\ &= \frac{1}{\|H(k,:)\|} \langle 2(\tilde{H}\tilde{H}^\top + \delta I)^{-1}\tilde{H}, E_{k,j} \rangle \\ &\quad - \frac{1}{\|H(k,:)\|} \langle 2(\tilde{H}\tilde{H}^\top + \delta I)^{-1}, e_k \tilde{H}(k,:)\tilde{H}^\top \rangle \tilde{H}(k,j). \end{aligned}$$

In the end,

$$\frac{\partial \log \det(\tilde{H}\tilde{H}^\top + \delta I)}{\partial H} = 2S^{-1} \left[(\tilde{H}\tilde{H}^\top + \delta I)^{-1} - \tilde{D}_\delta \right] \tilde{H}$$

and

$$\frac{\partial f}{\partial H} = W^\top (WH - X) - 2\lambda S^{-1} \left[(\tilde{H}\tilde{H}^\top + \delta I)^{-1} - \tilde{D}_\delta \right] \tilde{H},$$

where $\tilde{D}_\delta = \text{Diag} \left((\tilde{H}\tilde{H}^\top + \delta I)^{-1} \tilde{H}\tilde{H}^\top \right)$.

V. NUMERICAL EXPERIMENTS

In this section, we compare MinVol NMF, MaxVol NMF and N-MaxVol NMF on synthetic and hyperspectral datasets. The hyperparameter λ is again tuned using [21], as it has been specified in Remark 1

A. Synthetic datasets

The synthetic datasets are generated by mixing five endmembers from the USGS library. The ground truth W contains the spectral signature of these endmembers, displayed on Figure 7. We consider the two cases where W is well conditioned, leaving the endmembers as they are in Figure 7, and where W is ill conditioned, scaling its columns linearly from 0.05 to 1. The columns of the ground truth abundance matrix H are drawn following a Dirichlet distribution with parameter $\alpha = 0.1$, and clipping the values below 0.05 to zero. We consider the two cases where H is column-wise stochastic and where it is not, scaling its columns randomly, where the scaling follows a normal distribution $\mathcal{N}(1, 0.2^2)$. This simulates the presence of different lighting conditions. The data is generated as $X = WH + N$ where N is Gaussian noise. We consider three different signal-to-noise ratios (SNR): 30dB, 20dB and 10dB. For each of the four configurations,

we generate 20 noiseless different datasets WH and add the noise N afterward. The estimated W is compared to the ground truth W by computing the maximum angle between the matched ground truth and estimated endmembers. In other words, among the endmembers, how accurate is the least accurately estimated endmember. The results are displayed as box plots on Figure 8. As expected, N-MaxVol NMF outperforms MinVol NMF when H is not stochastic, while MaxVol performs best when H is stochastic followed by N-MaxVol NMF. This confirms our theoretical findings that MaxVol NMF is more suitable than MinVol NMF as it is not biased towards rank-deficient solutions while it allows to recover sparse H .

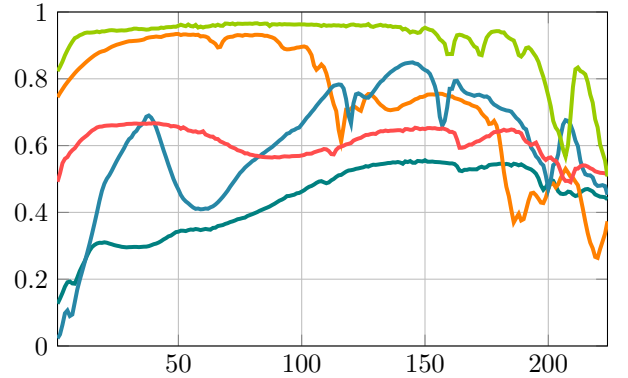


Figure 7: Spectral signature of five endmembers from the USGS library used to generate the synthetic datasets.

B. Hyperspectral images

Let us now evaluate the performance of N-MaxVol NMF on famous hyperspectral datasets. Results can be compared with [27] where some ground-truths for a variety of known hyperspectral datasets are proposed. Even if these are called ground-truths, hyperspectral ground-truths do not exist except if the measurements are performed in a controlled environment. Consider the proposed abundance maps for Urban with four endmembers in [27]. Clearly, some trees are detected where in fact it should be a mixture of grass and soil. Some rooftops are also detected where it should be soil. Still, the author used as many a priori knowledge as possible to provide these abundance maps and endmembers that are probably close to reality. Our message here is that ground-truths for these hyperspectral datasets should be interpreted with caution. On Moffett and on Samson, our model clearly outperforms MinVol NMF and MaxVol NMF, see Figures 9 and 10. Water, soil and tree are correctly separated and their spectral signatures are very close to the expected ones in [27]. The visual results for MinVol and MaxVol NMF for all data sets are provided in the Supplementary Material.

1) *Samson hyperspectral image*: Let us consider the Samson with $r = 6$, although Samson contains mostly 3 endmembers. With MinVol NMF, the 3 virtual endmembers are brought to zero by properly tuning λ and δ . On the other hand, using $r = 6$ allows MaxVol NMF to learn more spectral varieties; see Figure 11. We see three different kinds of tree and two

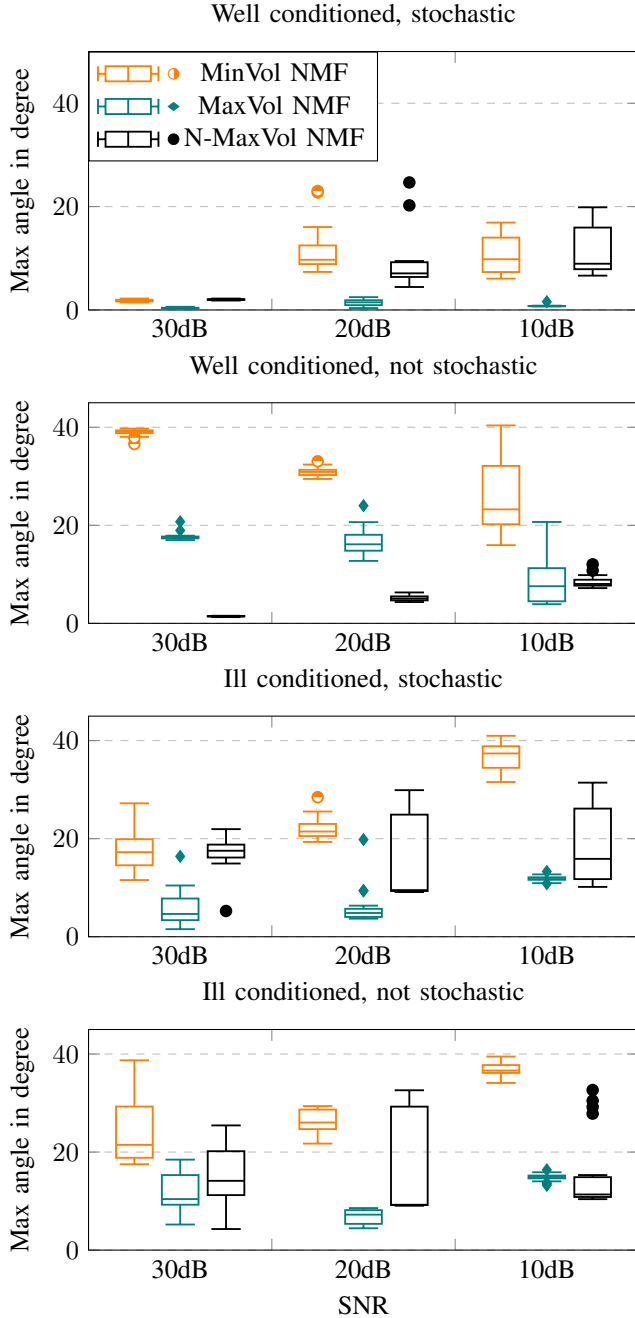


Figure 8: Box plots of the maximum angles between the ground truth and the estimated endmembers, depending on the model, the SNR and the configuration of W and H .

different kinds of soil. We can then add together the rows of H that correspond to varieties of the same endmembers. The resulting merged abundance maps are shown on Figure 12. The abundance maps on Figure 12 and Figure 10 are very close to each other. Actually, results with $r = 6$ are more satisfying for the water unmixing. On Figure 10, some small artifacts of false-positives can be seen, especially in the bottom right corner of the abundance map corresponding to water. These artifacts are not visible on Figure 12. This illustrates that MaxVol NMF allows us to increase the number of endmembers

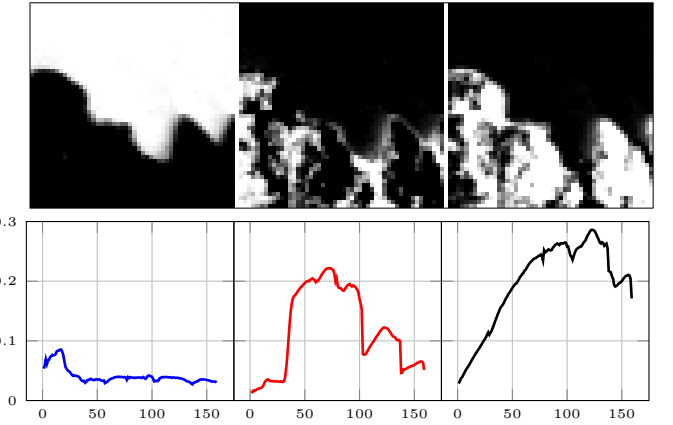


Figure 9: Abundance maps and endmembers (water, tree and soil) by N-MaxVol NMF on Moffett, with $\lambda = 1$ and $\delta = 0.5$.

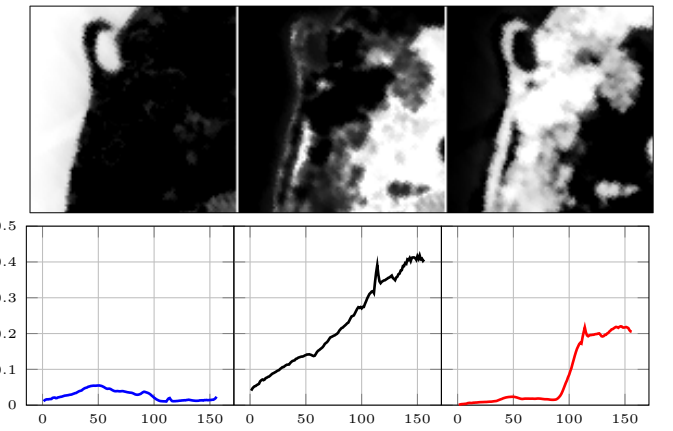


Figure 10: Abundance maps and endmembers (water, soil and tree) by N-MaxVol NMF on Samson, with $\lambda = 1$ and $\delta = 0.5$.

in order to improve the results in a controlled manner.

2) *Urban hyperspectral image:* The Urban datasets contains 162 spectral bands, and images of size 307×307 . It is the aerial photo of a Walmart in Texas. This dataset is particularly insightful because it is known for having meaningful unmixing results for $r = 4, 5$ and 6 [27]. Results are displayed on Figure 13. With $r = 4$, we have roof, grass, a combination of asphalt and soil, and tree. With $r = 5$, the distinction is being made between asphalt and dirt. With $r = 6$, the distinction is being made between grass and dry grass. Typical ground-truths with $r = 6$ rather suggest a distinction between two kinds of roofs, instead of grass and dry grass. Here our model propose another interpretation for $r = 6$ which makes sense.

3) *Jasper hyperspectral image:* The last experiment is on the Jasper dataset, where ground-truths suggest four endmembers: tree, water, soil and road. Unmixing algorithms often struggle to correctly separate water and road on Jasper. Figure 14 shows that N-MaxVol NMF achieves not ideal but nonetheless decent results. The issue with our model here is that in order to improve the distinction between water and road, λ should be increased. However, there are many areas where tree and soil are heavily mixed, and increasing λ will

associate these pixels with single endmember. One way to circumvent this issue is to increase the rank. Results with $r = 5$ are displayed on Figure 15. The additional endmember is in fact a combination of tree and soil. With this trick, water and road are properly identified without compromising the quality of the other endmembers.

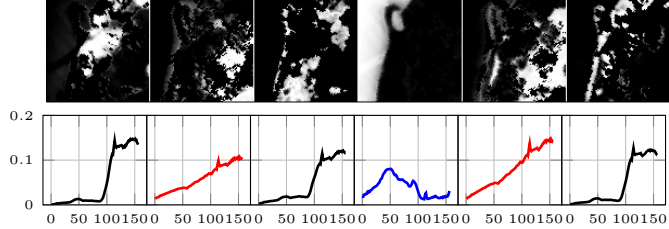


Figure 11: Abundance maps and endmembers (tree, **soil** and **water**) by N-MaxVol NMF with $r = 6$ on Samson, with $\lambda = 0.5$ and $\delta = 0.5$.

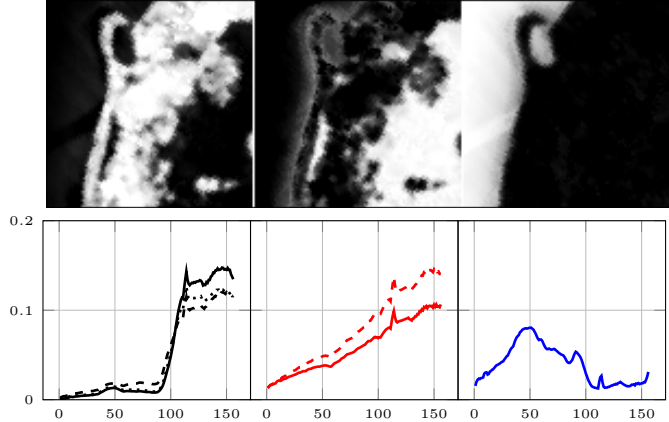


Figure 12: Abundance maps grouped by endmember varieties and endmembers (tree, **soil** and **water**) by N-MaxVol NMF with $r = 6$ on Samson, with $\lambda = 0.5$ and $\delta = 0.5$.

VI. CONCLUSION

In this paper, we first explored MaxVol NMF, a dual version of MinVol NMF, where the volume of H is maximized instead of the volume of W being minimized. In the noiseless case, MaxVol NMF is identifiable under the same conditions as MinVol NMF. In noisy settings, MaxVol NMF alleviates two important issues of MinVol NMF: the generation of rank-deficient solutions, and the difficulty to control the sparsity of H . We proposed two different algorithms to solve MaxVol NMF. A drawback of MaxVol NMF is that it tends to generate clusters of the same size. This motivated us to introduce normalized MaxVol NMF (N-MaxVol NMF), a variant where the volume of the row-wise normalized H factor is maximized. This model creates a continuum between NMF and ONMF, and leads to better separations than MinVol NMF on synthetic and hyperspectral unmixing.

Further research directions include the study of the identifiability of N-MaxVol NMF, and the use of N-MaxVol NMF on other types of data, e.g., document data sets or audio signals.

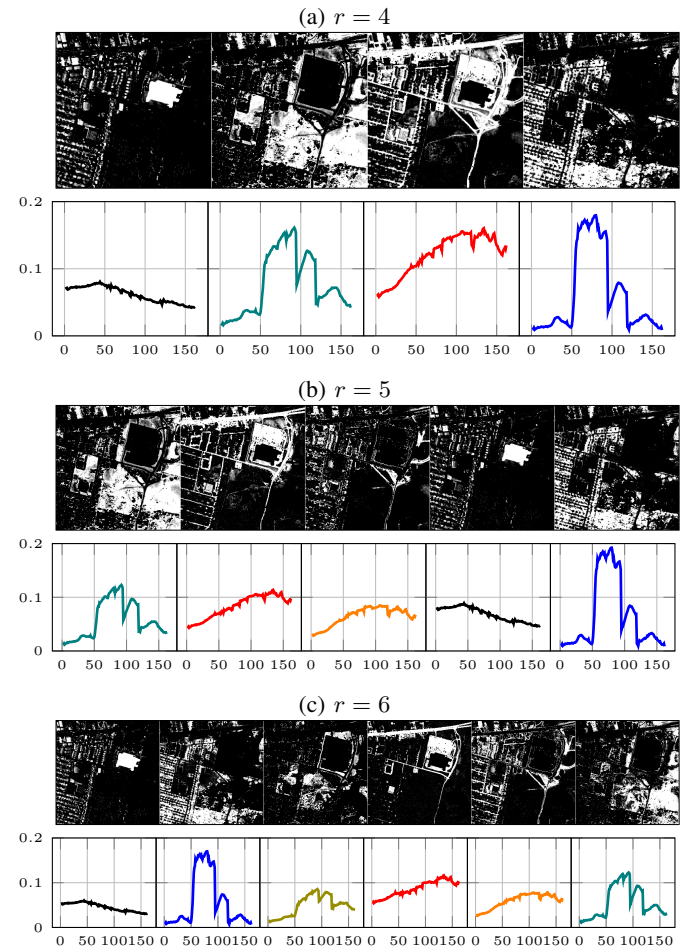


Figure 13: Abundance maps and endmembers (roof, **tree**, **dry grass**, **asphalt**, **soil**, **grass**) by N-MaxVol NMF on Urban, with $\lambda = 0.5$ and $\delta = 0.5$, depending on r .

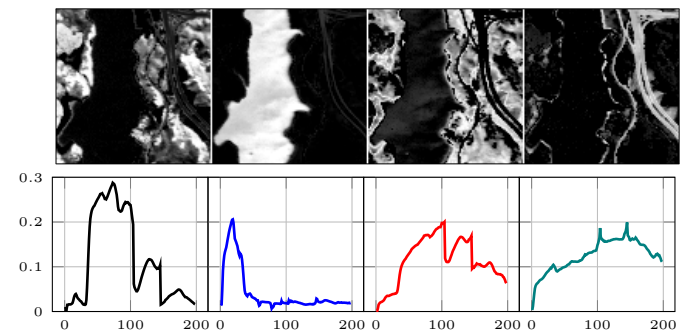


Figure 14: Abundance maps and endmembers (tree, **water**, **soil**, **road**) by N-MaxVol NMF with $r = 4$ on Jasper, with $\lambda = 2$ and $\delta = 1$.

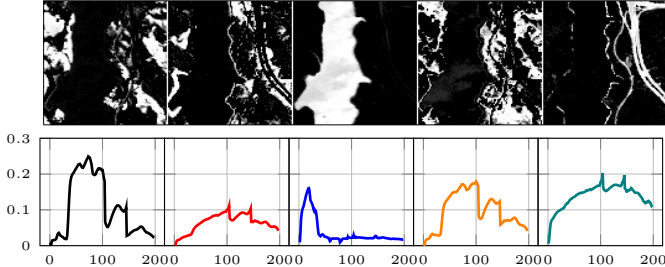


Figure 15: Abundance maps and endmembers (tree, soil, water, tree+soil, road) by N-MaxVol NMF with $r = 5$ on Jasper, with $\lambda = 0.5$ and $\delta = 0.5$.

APPENDIX A OPTIMAL HH^\top FOR MAXVOL NMF AS $\lambda \rightarrow \infty$

Let us introduce the notation $G = HH^\top \in \mathbb{S}^r$, where \mathbb{S}^r is the set of r -by- r symmetric matrices. Now consider

$$\begin{aligned} & \underset{G \in \mathbb{S}^r}{\text{minimize}} \quad f_0(G) = \log \det(G + \delta I)^{-1} \\ & \text{subject to} \quad e^\top G e \leq a, G \geq 0, \end{aligned} \quad (29)$$

where $a > 0$ and $\text{dom } f_0 = \{G \in \mathbb{S}^r, G \succ -\delta\}$. Note that $e^\top HH^\top e = n$. We prove that $G = \frac{a}{r}I$ is the unique minimizer of (29). To do so, we solve (29) through its dual using the conjugate of f_0 , as in [6, Section 5.1.6].

Definition 4: The conjugate f^* of a function $f : \mathbb{R}^r \rightarrow \mathbb{R}$ is given by

$$f^*(y) = \sup_{x \in \text{dom } f} (y^\top x - f(x)).$$

Considering the optimization problem with linear inequality and equality constraints

$$\min_x f_0(x) \quad \text{such that} \quad Ax \leq b, Cx = d, \quad (30)$$

the conjugate of f_0 can be used to write the dual function for (30) as

$$\begin{aligned} g(\lambda, \nu) &= \inf_x (f_0(x) + \lambda^\top (Ax - b) + \nu^\top (Cx - d)) \\ &= -b^\top \lambda - d^\top \nu + \inf_x (f_0(x) + (A^\top \lambda + C^\top \nu)^\top x) \\ &= -b^\top \lambda - d^\top \nu - f_0^*(-A^\top \lambda - C^\top \nu). \end{aligned} \quad (31)$$

The domain of g follows from the domain of f_0^* :

$$\text{dom } g = \{(\lambda, \nu) \mid -A^\top \lambda - C^\top \nu \in \text{dom } f_0^*\}.$$

Let us go back to the conjugate function of f_0 , which is defined as

$$f_0^*(Y) = \sup_{G \succ -\delta} (\langle Y, G \rangle + \log \det(G + \delta I)).$$

We first show that $\langle Y, G \rangle + \log \det(G + \delta I)$ is unbounded above unless $Y \prec 0$. If $Y \not\prec 0$, then Y has an eigenvector v , with $\|v\|_2 = 1$, and eigenvalue $\lambda \geq 0$. Taking $G = I + tvv^\top$

we find that

$$\begin{aligned} \langle Y, G \rangle + \log \det(G + \delta I) \\ &= \text{tr } Y + t\lambda + \log \det((1 + \delta)I + tvv^\top) \\ &= \text{tr } Y + t\lambda + r \log(1 + \delta) + \log \left(1 + \frac{t}{1 + \delta}\right) \end{aligned}$$

which is unbounded above as $t \rightarrow \infty$. Now consider the case $Y \prec 0$. We can find the maximizing G by setting the gradient with respect to G equal to zero:

$$\nabla_G (\langle Y, G \rangle + \log \det(G + \delta I)) = Y + (G + \delta I)^{-1} = 0,$$

which leads to $G = -Y^{-1} - \delta I$. Therefore, we have

$$f_0^*(Y) = \log \det(-Y)^{-1} - r - \delta \text{tr}(Y) \quad (32)$$

with $\text{dom } f_0^* = -\mathbb{S}_{++}^r$.

Applying the result in (31), the dual function for problem (29) is given by

$$g(\lambda, \nu) = \log \det(\lambda J - \nu) + r + \delta \text{tr}(\lambda J - \nu) - \lambda a$$

if $\lambda J - \nu \succ 0$, where $J = ee^\top$ is the matrix of all ones of appropriate dimension, and $g(\lambda, \nu) = \infty$ otherwise, with $\lambda \in \mathbb{R}_+$ and $\nu \in \mathbb{R}_+^{r \times r}$. Let

$$\lambda^* = \frac{r}{a} \left(1 + \frac{\delta}{\frac{a}{r} + \delta}\right), \quad \nu^* = \frac{r}{a} \left(1 + \frac{\delta}{\frac{a}{r} + \delta}\right) J - \frac{1}{\frac{a}{r} + \delta} I$$

and $G^* = \frac{a}{r}I$. We have $f_0(G^*) = g(\lambda^*, \nu^*) = -r \log(\frac{a}{r} + \delta)$, meaning that there is no duality gap and that G^* is a solution of (29). Finally, G^* is the unique solution because f_0 is strictly convex.

APPENDIX B OPTIMAL $\tilde{H}\tilde{H}^\top$ FOR MAXVOL NMF AS $\lambda \rightarrow \infty$

Let us introduce the variable $G = \tilde{H}\tilde{H}^\top$, and show that the problem

$$\begin{aligned} & \underset{G \in \mathbb{S}^r}{\text{minimize}} \quad f_0(G) = \log \det(G + \delta I)^{-1} \\ & \text{subject to} \quad \text{Diag}(G) = e, 0 \leq G \leq 1, \end{aligned} \quad (33)$$

where $\text{dom } f_0 = \mathbb{S}_{++}^r$, has $G = I$ as a unique minimizer. Again, we solve this problem through its dual using the conjugate of f_0 , which has already been computed in (32). First, (33) can be reformulated as

$$\begin{aligned} & \underset{G \in \mathbb{S}^r}{\text{minimize}} \quad f_0(G) = \log \det(G + \delta I)^{-1} \\ & \text{subject to} \quad \begin{aligned} & \langle E_{ii}, G \rangle = 1 \text{ for all } i, \\ & \langle -E_{ij}, G \rangle \leq 0 \text{ for all } i, j, \\ & \langle E_{ij}, G \rangle \leq 1 \text{ for all } i, j. \end{aligned} \end{aligned} \quad (34)$$

Using again (31), we can write the dual of (34) with the conjugate of f_0 :

$$\begin{aligned} g(\lambda, \gamma, \nu) &= \log \det(\text{Diag}(\nu) + \gamma - \lambda) - \langle J, \gamma \rangle - e^\top \nu \\ &\quad + r - \delta \text{tr}(\text{Diag}(\nu) + \gamma - \lambda) \end{aligned}$$

if $\text{Diag}(\nu) + \gamma - \lambda \succ 0$, and ∞ otherwise, where $\lambda \in \mathbb{R}_+^{r \times r}$, $\gamma \in \mathbb{R}_+^{r \times r}$ and $\nu \in \mathbb{R}^r$. Let $\lambda^* = 0, \gamma^* = 0, \nu^* = \frac{1}{1+\delta}e$ and

$G^* = I$. We have $f_0(G^*) = g(\lambda^*, \gamma^*, \nu^*) = -r \log(1 + \delta)$, meaning that there is no duality gap and that G^* is a solution of (33). Finally, G^* is the unique solution because f_0 is strictly convex.

Let us prove that the minimum of the volume criterion is reached when $\tilde{H}\tilde{H}^\top = J := ee^\top$ by solving

$$\begin{aligned} \text{minimize}_{G \in \mathbb{S}^r} \quad & f_1(G) = \log \det(G + \delta I) \\ \text{subject to} \quad & \langle E_{ii}, G \rangle = 1 \text{ for all } i, \\ & \langle -E_{ij}, G \rangle \leq 0 \text{ for all } i, j, \\ & \langle E_{ij}, G \rangle \leq 1 \text{ for all } i, j. \end{aligned} \quad (35)$$

Skipping the details, the conjugate of f_1 is

$$f_1^*(Y) = r - \delta \operatorname{tr}(Y) + \log \det(Y)$$

with $\operatorname{dom} f_1^* = \mathbb{S}_{++}^r$. From (31), the dual g of (35) is

$$\begin{aligned} g(\lambda, \gamma, \nu) = \delta \operatorname{tr}(\lambda - \gamma - \operatorname{Diag}(\nu)) - \log \det(\lambda - \gamma - \operatorname{Diag}(\nu)) \\ - \langle J, \gamma \rangle - e^\top \nu - r \end{aligned}$$

if $\lambda - \gamma - \operatorname{Diag}(\nu) \succ 0$, and ∞ otherwise, where $\lambda \in \mathbb{R}_+^{r \times r}$, $\gamma \in \mathbb{R}_+^{r \times r}$ and $\nu \in \mathbb{R}^r$. Let $\lambda^* = 0$, $\gamma^* = \frac{1}{\delta(r+\delta)}J$, $\nu^* = -\frac{1}{\delta}e$ and $G^* = J = ee^\top$. We have $f_1(G^*) = g(\lambda^*, \gamma^*, \nu^*) = \log((r+\delta)\delta^{r-1})$, meaning that there is no duality gap and that G^* is a solution of (33). Finally, G^* is the unique solution because it is a vertex of the polyhedral set defined by the constraints in (35), and that the minimum of a strictly concave function like f_1 in a polyhedral set is reached on one the vertex of this set.

REFERENCES

- [1] M. Abdolali, G. Barbarino, and N. Gillis. Dual simplex volume maximization for simplex-structured matrix factorization. *SIAM Journal on Imaging Sciences*, 17(4):2362–2391, 2024.
- [2] A. M. S. Ang and N. Gillis. Algorithms and comparisons of nonnegative matrix factorizations with volume regularization for hyperspectral unmixing. *IEEE J. Sel. Top. Appl. Earth Obs. Remote Sens.*, 12(12):4843–4853, 2019.
- [3] H. H. Bauschke, J. Bolte, and M. Teboulle. A descent lemma beyond lipschitz gradient continuity: first-order methods revisited and applications. *Mathematics of Operations Research*, 42(2):330–348, 2017.
- [4] D. P. Bertsekas. Nonlinear programming: 3rd edition. 2016.
- [5] J. M. Bioucas-Dias, A. Plaza, N. Dobigeon, M. Parente, Q. Du, P. Gader, and J. Chanussot. Hyperspectral unmixing overview: Geometrical, statistical, and sparse regression-based approaches. *IEEE J. Sel. Top. Appl. Earth Obs. Remote Sens.*, 5(2):354–379, 2012.
- [6] S. Boyd, S. P. Boyd, and L. Vandenberghe. *Convex optimization*. Cambridge university press, 2004.
- [7] L. Condat. Fast projection onto the simplex and the l_1 ball. *Mathematical Programming*, 158(1-2):575–585, 2016.
- [8] M. D. Craig. Minimum-volume transforms for remotely sensed data. *IEEE Trans. Geosci. Remote Sens.*, 32(3):542–552, 1994.
- [9] R.-A. Dragomir, A. d’Aspremont, and J. Bolte. Quartic first-order methods for low-rank minimization. *Journal of Optimization Theory and Applications*, 189:341–363, 2021.
- [10] X. Fu, K. Huang, N. D. Sidiropoulos, Q. Shi, and M. Hong. Anchor-free correlated topic modeling. *IEEE Transactions on Pattern Analysis and Machine Intelligence*, 41(5):1056–1071, 2018.
- [11] X. Fu, K. Huang, B. Yang, W.-K. Ma, and N. D. Sidiropoulos. Robust volume minimization-based matrix factorization for remote sensing and document clustering. *IEEE Trans. Signal Process.*, 64(23):6254–6268, 2016.
- [12] X. Fu, W.-K. Ma, K. Huang, and N. D. Sidiropoulos. Blind separation of quasi-stationary sources: Exploiting convex geometry in covariance domain. *IEEE Trans. Signal Process.*, 63:2306–2320, 2015.
- [13] W. E. Full, R. Ehrlich, and J. Klovan. EXTENDED QMODEL—objective definition of external end members in the analysis of mixtures. *Journal of the International Association for Mathematical Geology*, 13(4):331–344, 1981.
- [14] M. Held, P. Wolfe, and H. P. Crowder. Validation of subgradient optimization. *Mathematical programming*, 6:62–88, 1974.
- [15] L. T. K. Hien, D. N. Phan, and N. Gillis. An inertial block majorization minimization framework for nonsmooth nonconvex optimization. *Journal of Machine Learning Research*, 24:1–41, 2023.
- [16] D. D. Lee and H. S. Seung. Learning the parts of objects by non-negative matrix factorization. *Nature*, 401:788–791, 1999.
- [17] V. Leplat, A. M. S. Ang, and N. Gillis. Minimum-volume rank-deficient nonnegative matrix factorizations. In *ICASSP*, pages 3402–3406, 2019.
- [18] V. Leplat, N. Gillis, and M. S. Ang. Blind audio source separation with minimum-volume beta-divergence NMF. *IEEE Transactions on Signal Processing*, 68:3400–3410, 2020.
- [19] C.-H. Lin, W.-K. Ma, W.-C. Li, C.-Y. Chi, and A. Ambikapathi. Identifiability of the simplex volume minimization criterion for blind hyperspectral unmixing: The no-pure-pixel case. *IEEE Trans. Geosci. Remote Sens.*, 53(10):5530–5546, 2015.
- [20] Y. Malitsky and K. Mishchenko. Adaptive gradient descent without descent. In *Proceedings of the 37th International Conference on Machine Learning*, ICML’20. JMLR.org, 2020.
- [21] D. T. Nguyen and E. C. Chi. Towards tuning-free minimum-volume nonnegative matrix factorization. In *Proceedings of the 2024 SIAM International Conference on Data Mining (SDM)*, pages 217–225. SIAM, 2024.
- [22] F. Pompili, N. Gillis, P.-A. Absil, and F. Glineur. Two algorithms for orthogonal nonnegative matrix factorization with application to clustering. *Neurocomputing*, 141:15–25, 2014.
- [23] G. Tatli and A. T. Erdogan. Polytopic matrix factorization: Determinant maximization based criterion and identifiability. *IEEE Trans. Signal Process.*, 69:5431–5447, 2021.
- [24] O. Vu Thanh, A. Ang, N. Gillis, and L. T. K. Hien. Inertial majorization-minimization algorithm for minimum-volume nmf. In *European Signal Processing Conference (EUSIPCO)*, pages 1065–1069, 2021.
- [25] C. Wang, D. Sun, and K.-C. Toh. Solving log-determinant optimization problems by a newton-cg primal proximal point algorithm. *SIAM Journal on Optimization*, 20(6):2994–3013, 2010.
- [26] J. Wang, S. Guan, S. Liu, and X.-L. Zhang. Minimum-volume multichannel nonnegative matrix factorization for blind audio source separation. *IEEE/ACM Transactions on Audio, Speech, and Language Processing*, 29:3089–3103, 2021.
- [27] F. Zhu. Hyperspectral unmixing: ground truth labeling, datasets, benchmark performances and survey. *arXiv preprint arXiv:1708.05125*, 2017.

SUPPLEMENTARY MATERIAL

In this Supplementary Material, we report the results for MinVol NMF and MaxVol NMF on data sets which are not included in the paper. The parameters for these two models, namely λ and δ , were chosen to achieve good results. Table II summarizes the content of these figures.

	Moffet	Samson	Urban	Jasper
MinVol NMF	Fig. 16	Fig. 18	Fig. 20	Fig. 22
MaxVol NMF	Fig. 17	Fig. 19	Fig. 21	Fig. 23

Table II: Content of this Supplementary Material: results from MinVol and MaxVol NMF on four data sets.

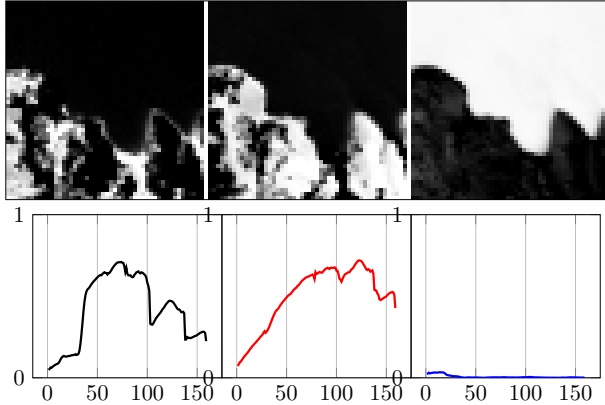


Figure 16: Abundance maps and endmembers (tree, **soil** and **water**) by MinVol NMF on Moffett, with $\lambda = 1$ and $\delta = 0.5$.

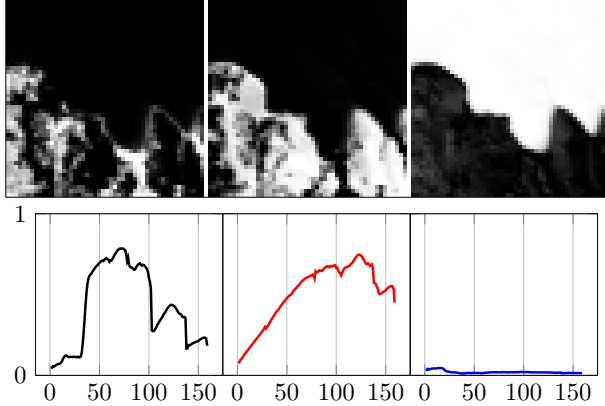


Figure 17: Abundance maps and endmembers (tree, **soil** and **water**) by MaxVol NMF on Moffett, with $\lambda = 1$ and $\delta = 1$.

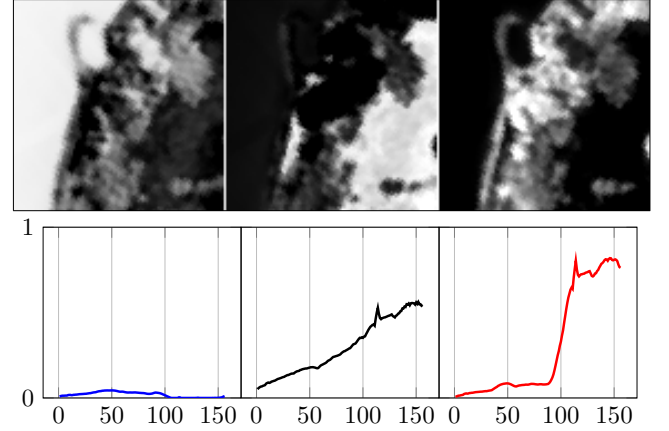


Figure 18: Abundance maps and endmembers (**water**, soil and **tree**) by MinVol NMF on Samson, with $\lambda = 1$ and $\delta = 0.5$.

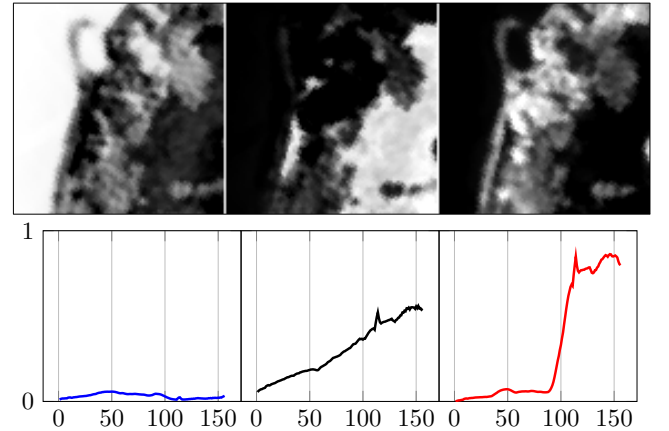


Figure 19: Abundance maps and endmembers (**water**, soil and **tree**) by MaxVol NMF on Samson, with $\lambda = 1$ and $\delta = 1$.

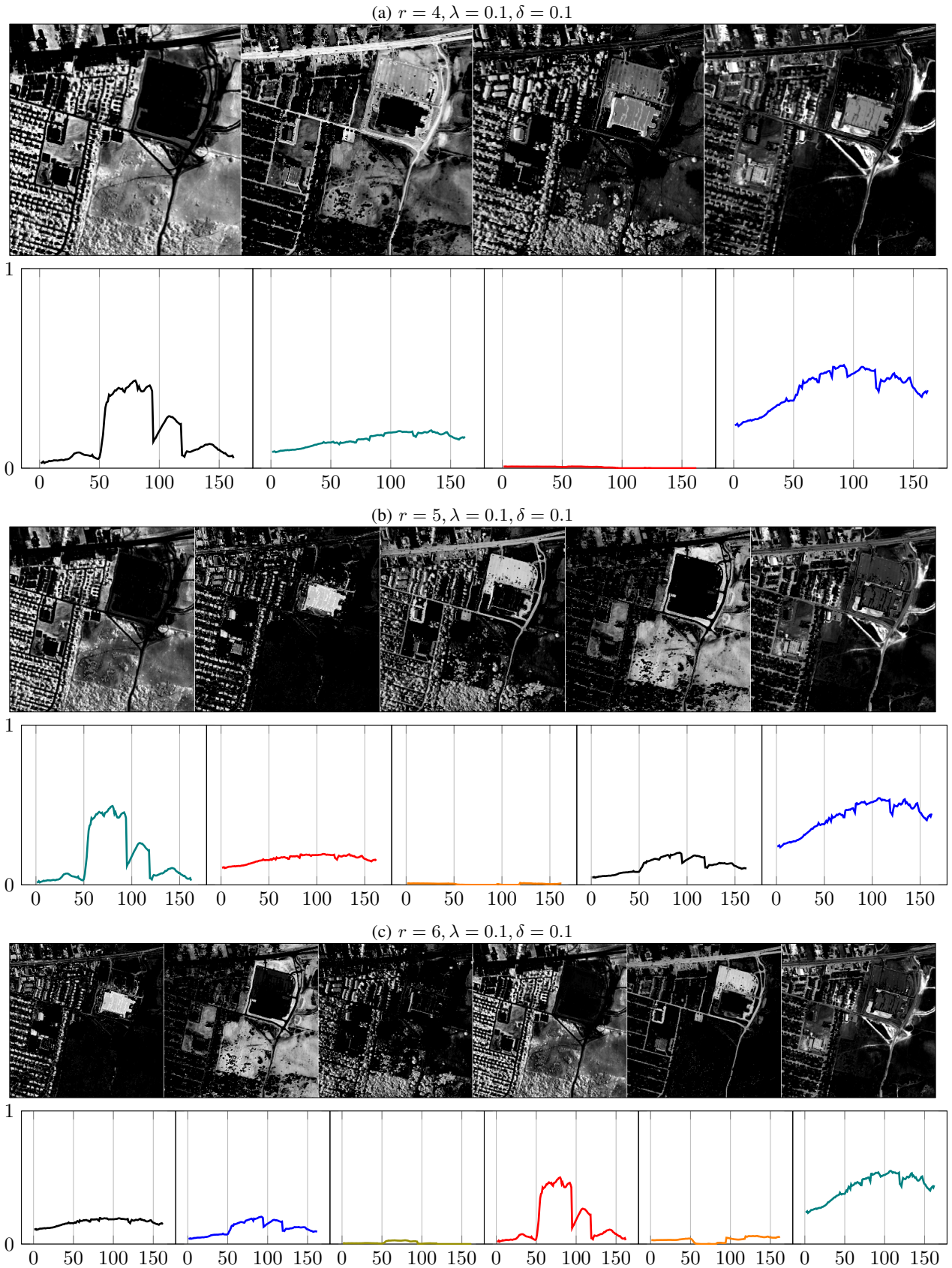


Figure 20: Abundance maps and endmembers by MinVol NMF on Urban, depending on r , λ and δ .

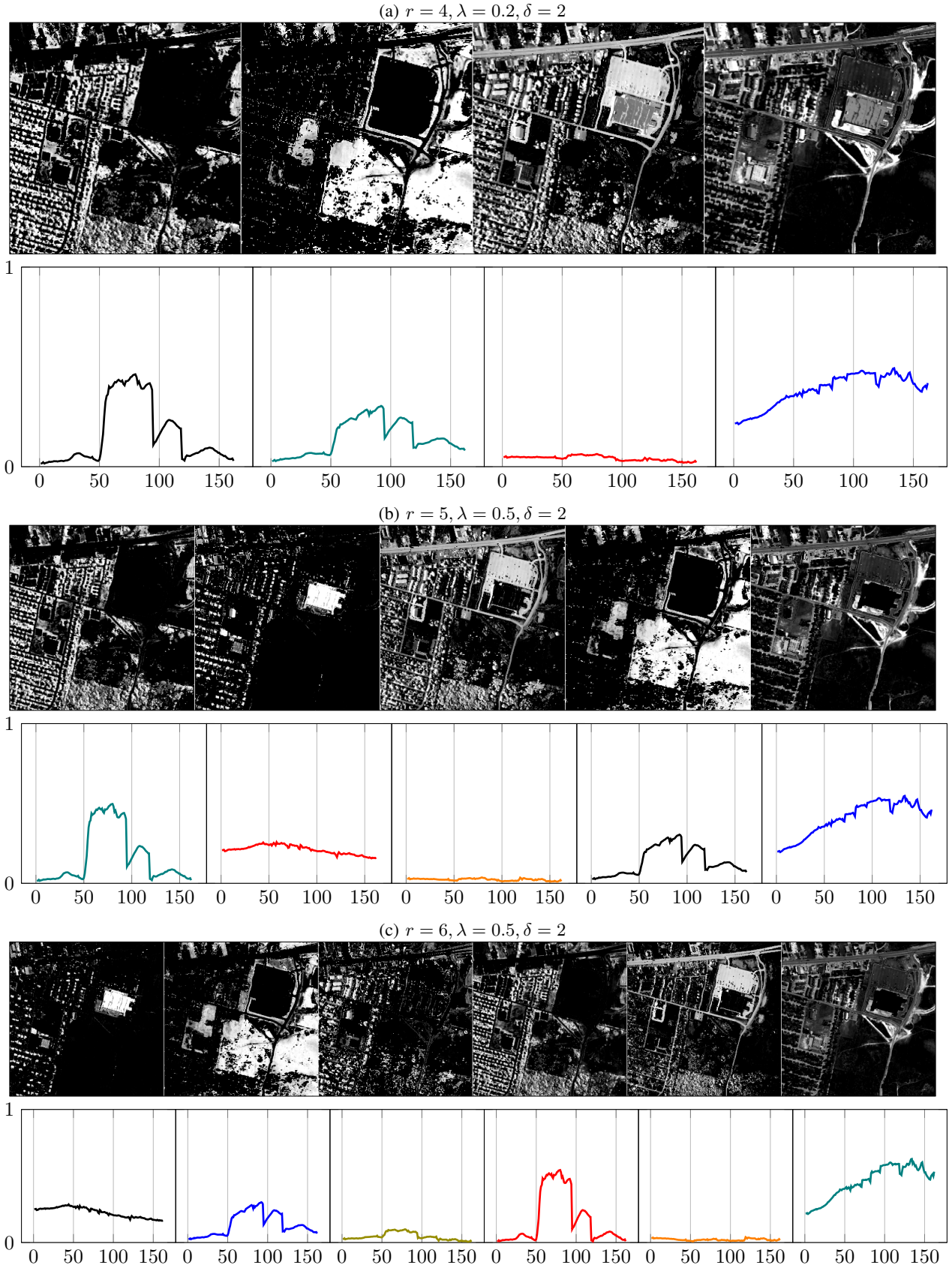


Figure 21: Abundance maps and endmembers by MaxVol NMF on Urban, depending on r , λ and δ .

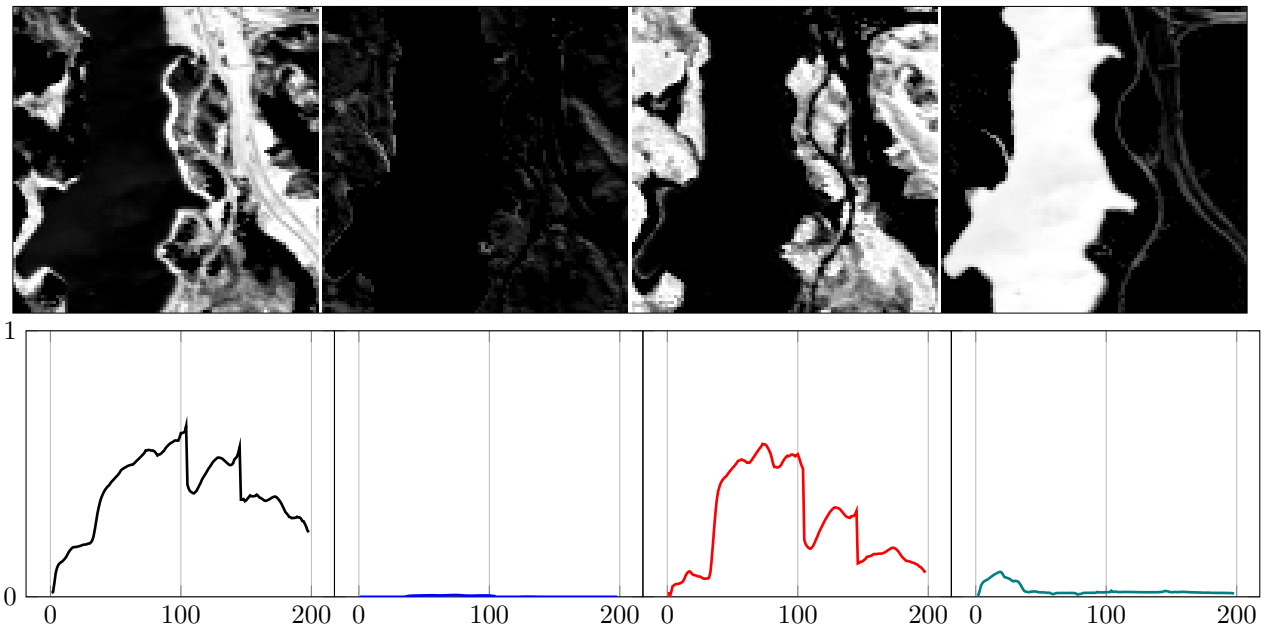


Figure 22: Abundance maps and endmembers (road and soil, **tree and soil**, **water**) by MinVol NMF with $r = 4$ on Jasper, with $\lambda = 0.5$ and $\delta = 1$.

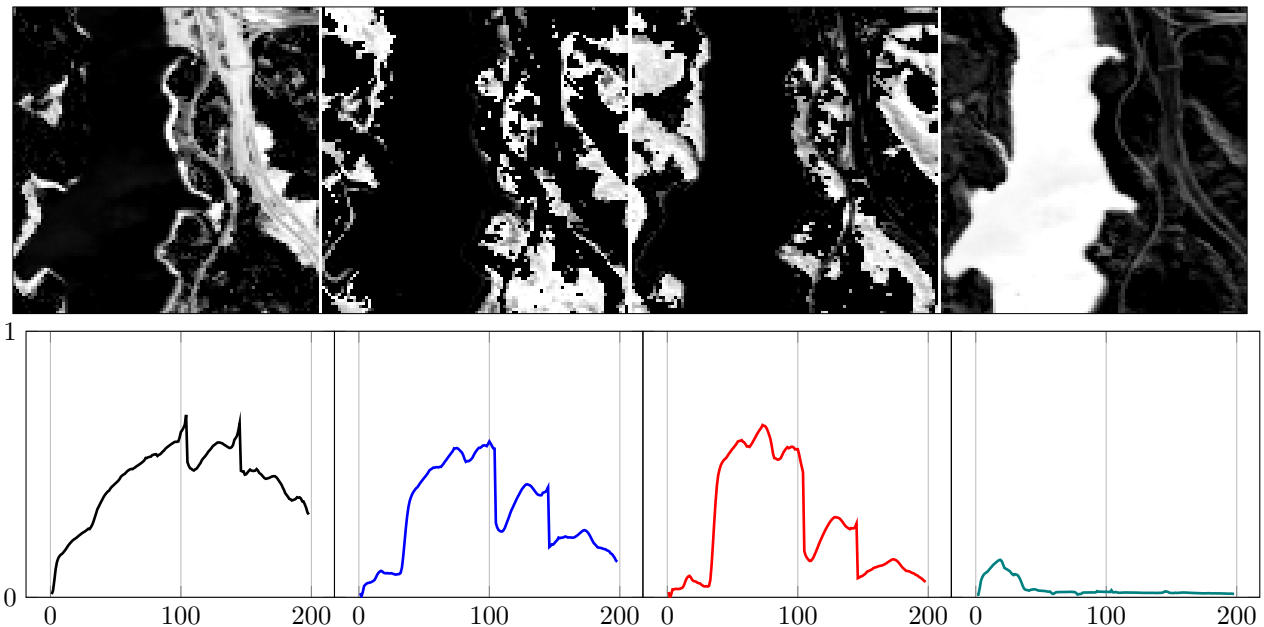


Figure 23: Abundance maps and endmembers (road, **tree and soil**, **tree**, **water**) by MaxVol NMF with $r = 4$ on Jasper, with $\lambda = 0.5$ and $\delta = 1$.